Differences in the structure of plant polygalacturonases specify enzymes' dynamics and processivities to fine-tune pectins and root development

Josip Safran[1#], Wafae Tabi[1#], Vanessa Ung[2#], Adrien Lemaire[1], Olivier Habrylo[1], Julie Bouckaert[3], Maxime Rouffle[1], Aline Voxeur[4], Paula Pongrac[1], Solène Bassard[1], Roland Molinié[1], Jean-Xavier Fontaine[1], Serge Pilard[5], Corinne Pau-Roblot[1], Estelle Bonnin[6], Danaé Sonja Larsen[2], Mélanie Morel-Rouhier[7], Jean-Michel Girardet[7], Valérie Lefebvre[1], Fabien Sénéchal[1§], Davide Mercadante[2§], Jérôme Pelloux[1§]

[1]UMRT INRAE 1158 BioEcoAgro – BIOPI Biologie des Plantes et Innovation, Université de Picardie, 33 Rue St Leu, 80039 Amiens, France. [2]School of Chemical Sciences, The University of Auckland, Private Bag 92019, Auckland 1142, New Zealand. [3]UMR 8576 Unité de Glycobiologie Structurale et Fonctionnelle (UGSF), 50 Avenue de Halley, 59658 Villeneuve d'Ascq, France. [4]Université Paris-Saclay, INRAE, AgroParisTech, Institut Jean-Pierre Bourgin (IJPB), 78000, Versailles, France [5]Plateforme Analytique, Université de Picardie, 33, Rue St Leu, 80039 Amiens, France. [6]INRAE, UR 1268 Biopolymers, Interactions Assemblies, CS 71627, 44316 Nantes Cedex 3, France. [7]Université de Lorraine, INRAE, IAM, F-54000 Nancy, France.

#: Contributed equally as first authors

§: Contributed equally as last authors

Corresponding authors:

Jérôme Pelloux (jerome.pelloux@u-picardie.fr)

Davide Mercadante (davide.mercadante@auckland.ac.nz)

Fabien Sénéchal (fabien.senechal@u-picardie.fr)

Abstract

The fine-tuning of pectins by polygalacturonases (PGs) plays a key role in modulating plant cell wall chemistry and mechanics, impacting plant development. The high number of plant PG isoforms and their absence of inhibition by endogenous PG-Inhibiting Proteins (PGIPs) question the regulation of pectin depolymerization during development. Our understanding of the diversity and of the regulation of plant PGs has been impaired by the lack of protein structures. Here we resolved the crystal structures of two PGs from Arabidopsis, PGLR and ADPG2, whose expression overlap in roots and determined why plant PGs are not inhibited by PGIPs. By combining molecular dynamic simulations, analysis of enzymes' kinetics and hydrolysis products, we showed that subtle differences in PGLR and ADPG2 structures translated into distinct dynamics and processivities. This leads to peculiar effects on root development, as determined by exogenous applications of enzymes.

Introduction

The plant primary cell wall, composed of an intricate network of polysaccharides and proteins, is constantly remodelled translating in changes in its mechanical properties, which ultimately affect the extent of cell growth or the response to environmental stress[1]. Pectin, the major polysaccharide of the primary cell wall of dicotyledonous species such as Arabidopsis, are composed of homogalacturonan (HG): a homopolymer of α-1,4-linked-D-galacturonic acid (GalA) units, that can be substituted with methylester and/or acetyl groups[2]. The control of the degree of polymerization (DP) of HG by polygalacturonases (PGs) regulates diverse developmental processes such as root/hypocotyl growth, stomata functioning, cell separation during pollen formation and pollen tube elongation[3–8]. Importantly, phytopathogenic organisms, including parasitic plants, also produce PGs, thus contributing to host colonization by degrading the physical barrier of the plant cell wall[9]. Although all perform the hydrolysis of the α-(1–4) glycosidic bond between two adjacent non-methylesterified GalA units, PGs can differ in their mode of action and are referred to as endo-PGs (EC 3. 2.1.15) or exo-PGs (EC 3.2.1.67) if they either hydrolyze in the middle of the HG chain or attack from the non-reducing end of it. All resolved structures of PGs from microorganisms fold into a right-handed parallel beta-helix and harbour four conserved amino acids (aa) stretches in their active site: namely NTD, DD, GHG and RIK[10]. In a typical endo-PG, such as that from *Aspergillus aculeatus* PG1 (AaPG1), the active site is organized in a tunnel-like binding cleft, allowing the enzyme to bind the polysaccharide and produce oligogalacturonides (OGs) of various DP and with different chemistries[11]. In contrast, the structure of exo-PGs differs, loop extension turns the open-ended channel into a closed pocket, restricting the attack to the non-reducing end of the substrate, and releasing non-methylesterified GalA monomers or dimers[12]. It has been reported that pathogenic PGs are inhibited by Polygalaturonase Inhibiting Proteins (PGIPs), expressed by plants upon infection, either through competitive or non-competitive interactions, in a strategic attempt by plants to limit pectin degradation and pathogenic invasion[13]. In contrast, plant PGs are not inhibited by PGIPs, which suggests yet unidentified structural differences among this class of enzymes. The PG-mediated degradation of HG can have two distinct consequences: i) it can impact polysaccharide rheology, decreasing cell wall stiffness and promoting cell growth (or infection by pathogens) and/or ii) it can produce OGs, which can act as signalling molecules[14,15]. It seems likely that the fine composition of OG arrays produced by a myriad of differentially expressed PG isoforms can modulate the oligosaccharide interactions with cell wall integrity receptors, triggering distinct downstream signalling events.

In plants, PGs are encoded by large multigenic families (68 genes in *Arabidopsis thaliana*), which questions the rationale for such an abundance in the context of the cell wall. Considering such a large number of genes, and potential compensation mechanisms mediated by partial functional redundancy between isoforms, the use of reverse or forward genetic mutants can only bring partial clues to sample the diversity of the plant PGs' landscape.

Here we report on the biochemical and first structural characterization of two plant PGs, PGLR (PolyGalacturonase Lateral Root) and ADPG2 (Arabidopsis Dehiscence zone PolyGalacturonase 2), whose expression overlaps in Arabidopsis roots during lateral root emergence[8,16]. We found that, although having an overall conserved structure and overlapping functional profiles, enzymes have key and noticeable differences in their mode of action, resulting in phenotypical differences on root growth. The investigation of PGLR and ADPG2 crystal structures, together with enzyme-substrate complexes, via combined experimental and computational approaches, including binding kinetics, Molecular Dynamics (MD) simulations, LC-MS/MS profiling of digestion products highlighted the existence of a direct link between enzyme-substrate interactions and dynamics, enzyme activities and specificities.

Overall, structural and dynamical analyses of PGLR and ADPG2 reported distinct dynamical behaviours, which led to the production of distinct OG pools. This shows that, despite apparent gene redundancy, plant PGs have distinct activities and processivities leading to peculiar consequences on plant development, as determined by the exogenous application of the enzymes during the early stages of seedlings development.

Results

Crystal structures of *A. thaliana* PGLR and ADPG2 reveals conserved β-fold

ADPG2 was produced as an active recombinant proteins in the yeast *Pichia pastoris* and subsequently purified, similarly to PGLR[8]. PGLR and ADPG2 present similar biochemical characteristics, with an optimal activity at acidic pH, temperatures ranging from 25 to 50 °C and on pectic substrates with low degree of methylesterification (DM, Extended data Fig. 1and ref.[8]). Using PGA as a substrate, at 25°C, PGLR and ADPG2 differ in their Km (14.57 versus 3.0 $mg.ml^{-1}$) and Vmax (30.8 versus 391.7 nmol of $GalA.min^{-1}.\mu g^{-1}$). Protein structures were determined by X-Ray crystallography with the final models' geometry, processing and refinement statistics summarized in Table 1. We solved the crystal structure of PGLR (429 aa , 1-18 and 409-429 aa not modelled, PDB: 7B7A) at a resolution of 1.3 Å using molecular replacement with 1RMG[17] (Fig. 1A, Extended data Fig. 2A). PGLR crystallised as a single molecule in a P1 asymmetric unit. The crystal structure of ADPG2 (420 aa, 1-41 and 406-420 aa not modelled, PDB: 7B8B) was resolved at a resolution of 2.0 Å using PGLR as the search model (Fig. 1A, Extended data Fig. 2B). ADPG2 crystals belonged to the orthorhombic space group $P2_12_12_1$ with chains A and B having a Cα root mean square deviation (rmsd) of 0.924 Å. PGLR and ADPG2 fold in right-handed parallel β-helical structure, which is common to pectinases (Fig. 1A)[11]. This β-helix is formed by three repeating parallel β-sheets - PB1, PB2 and PB3 which contain 11, 12, and 11 parallel β-strands respectively, as well as a small β-sheet, PB1a, having only 3 β-strands (Extended data Fig. 3A-B). T1-turns, T1a-turns, T2-turns and T3-turns connect the PB1-PB2, PB1-PB1a, PB2-PB3 and PB3-PB1 β-sheets, respectively (Extended data Fig. 3C-D)[18]. PGLR and ADPG2 show a α-helix at the N-terminus, interacting with the T1 turn through the establishment of a disulphide bridge (PGLR, C46-C76, ADPG2, C71-C98), which shields the hydrophobic core of the enzyme[19]. Superimposition of PGLR and ADPG2 structures resulted in a rmsd of 2.299 Å, predominantly due to a deviation in the region surrounding the active site, in particular N130–P142 (T3 turn, PGLR numbering) and Y304-V318 (T1a turn, PGLR numbering). Between these loops, a large cleft (10.29 Å wide for PGLR and 14.46 Å for ADPG2), open at both sides is present, exposing PB1 for accommodating the substrate and identifying PGLR and ADPG2 as putative endo-PGs[8,11,12].

Structural determinants of absence of plant PG-plant PGIP interactions

While PGLR and ADPG2 show low sequence identity with fungal enzymes (sequence identity: 19%-25% with AaPG1, AnPG1, AnPGII, FpPG1, PcPG1, CpPG1), they show high structural similarity with a rmsd of 4.753 to 7.761 Å between all atoms (Extended data Fig. 4A-

B). Still, PGLR does not interact with plant PGIPs, as shown by the lack of inhibition of PGLR activity by *Phaseolus vulgaris* PGIP2 (PvPGIP2)[8], while this interaction exists with fungal PGs[8,20]. To understand the structural basis of this absence of inhibition of plant PG activity by PGIP we superimposed the resolved structures of PGLR and ADPG2 onto the *Fusarium phyllophilum* PG (FpPG1) - PvPGIP2 complex (Fig. 1B)[13,20]. In FpPG1, a S120-N121-S122-N123 stretch, within the protein's N-terminal loop, plays a key role in the PG-PGIP interaction (N121 notably interacting with H110 of PvPGIP2). PGLR and ADPG2 N-terminal loops are, on the other hand, rich in bulkier and chemically different residues, including M132, M133 and M137 for PGLR and K160, K162 and K166 for ADPG2 (Extended data Fig. 5). At the C-terminus, A274, the aa that contributes to hydrophobic-stabilizing interactions for the FpPG1-PGIP is replaced by G277/G278 and G303/G304 in PGLR and ADPG2, respectively (Fig. 1C)[20]. Moreover, plant PGs have a specific H to P (P190/P216) substitution together with W275/Y301 insertion which can hinder the PG-PGIP interaction[21]. We next modelled AtPGIP1 and AtPGIP2, which superimpose to PvPGIP2 with a rmsd of 1.194 and 1.201 Å, respectively (Fig. 1D). The analysis of the models for PGLR/ADPG2-AtPGIP1/AtPGIP2 complexes showed that multiple aa are involved in steric clashes (between 81 and 275 atom contacts depending of the PG-PGIP pair, Supplementary data File 1), which, together with the above-mentioned structural features, can explain the absence of the interaction between AtPGs and endogenous AtPGIPs, and lack of protein-mediated inhibition of PG activity in planta (Fig. 1E, Extended data Fig. 6A-B).

PGs with conserved active sites show differences alongside the binding groove subsites known to be of importance for substrate interaction and processivity

Comparison of PGLR and ADPG2 sequences and structures with that from bacteria and fungi reveal that the active site is formed by four conserved structural motifs NTD, DD, GHG, RIK positioned at subsites -1 and +1 of the PB1[22–24]. Eight of these aa N191/N217, D193/D219, H196/H222 D214/D240, D215/D241, H237/H263, R271/R297, K273/K299 (PGLR/ADPG2 numbering) are strictly conserved with the three aspartates responsible for the hydrolysis of the substrate (Fig. 2A)[10,19,23,25]. To determine the importance of specific aa, five site-directed mutations were designed for PGLR: D215A occurring in the active site, R271Q (subsite +1), and the histidine mutants H196K, (subsite -1), H237K (subsite +1) and H196K/H237K (Extended data Fig. 7). Histidine residues could potentially modulate the activity of the enzyme by controlling the protonation state of residues placed in subsites flanking the hydrolysis site (Fig. 2A). Their activities, on PGA, and binding affinities (Kd) to the substrate (represented by

a mix of OGs of mean DP12 and DM5 and on which PGLR shows activity (Extended data Fig. 8) were determined by MicroScale Thermophoresis (MST). D215A and R271Q mutations resulted in a total loss of activity with a substantial reduction in binding affinity (Kd of 2567 µM and 4840 µM for D215A and R271Q, respectively compared to 1246 µM for WT, Fig. 2B). While binding affinities of all histidine mutants were not significantly different, the H237K and H196K/H237K mutants showed no residual activity while the H196K mutant had featured only 22% residual activity of the WT. Although having conserved active sites, sequence and structure analyses showed that twelve aa positioned alongside the binding groove (subsites from -5 to +5), previously shown to be of importance for substrate interaction and processivity differ between PGLR and ADPG2 (Fig. 2C-D) but as well with those of the fungal AaPG1 (Extended data Fig. 9)[11,22,24]. For instance, at subsite -5, PGLR harbours R146, that can be responsible for the interaction with a carboxylate group of GalA, while ADPG2 harbours T172. Similarly, at subsite -4, Q198 in PGLR is replaced by T224 in ADPG2. At subsite -4, -3 and -2 a patch formed by Q198, Q220 and the positively charged K246 in PGLR is mutated into T224, E246 and D272 in ADPG2. At subsite -1 S269 in ADPG2, that can form hydrogen bonds with the substrate is mutated into G243 in PGLR. Finally, at subsite +2 and +3 D293 and K322 in ADPG2 are replaced by T267 and A296 in PGLR.

Molecular dynamic (MD) simulations reveal distinct substrate-dependent dynamics of PGLR and ADPG2

The large number and chemical diversity of interactions across the binding groove make structural comparisons between different PG isoforms poorly informative. Such a diversity can result in different dynamic behaviours of enzymes and/or substrates, which could translate into different functional profiles. We performed MD simulations on PGLR and ADPG2 in complex with either a fully de-methylesterified (pattern 1) or 60% methylesterified (pattern 2) decasaccharides (Fig. 2E), able to occupy the totality of the binding groove (subsites from -5 to +5). We first simulated PGLR, PGLR H196K and H237K mutants in complex with fully de-methylesterified decasaccharides, and the analysis of substrate dynamics, through the quantification of subsite-specific root mean square fluctuations (RMSF), revealed a trend between enzymatic activity (Fig. 2B), substrate dynamics (Fig. 2F-H) and the total number of contacts between the substrate and enzymes (Extended data Fig. 10). MD simulations of the PGLR mutants (H196K and H237K) revealed how substrate dynamics is affected all along the binding groove, even with a single histidine mutation occurring in subsites either towards the non-reducing end (H196K – subsite -1) or the reducing end of the sugar (H237K – subsite +1).

Overall, a rigidification of the substrate coincides with the loss of activity observed in experiments (Fig. 2B), with the H237K mutant (total loss of activity) showing the lowest RMSF in subsites -1 to +5 compared to the H196K (22% residual activity) and the WT (highest substrate dynamics, Fig. 2G-H).

The substrate dynamics can be also seen when comparing the RMSF of ADPG2 and PGLR when in complex with either de-methylesterified or methylesterified decasaccharides. For both enzymes, de-methylesterified oligomers are overall less dynamic, hence more tightly bound in the binding groove (Fig. 3A-B). Quantitative differences in the RMSF of the two complexes suggest that, for the same substrate either being de-methylesterified or partially methylesterified, the binding to PGLR is tighter. Moreover, for each substrate, ADPG2 retains a higher activity compared to PGLR (Extended data Fig. 1E), which again corroborates the observation that methylesterified substrates are overall less dynamic in complex with PGLR when compared to ADPG2 (Fig. 3A-B). The observed substrate dynamics is linked to the total number of contacts with the enzyme, with some noticeable differences between the two isoforms. When in complex with de-methylesterified substrates, both enzymes establish a larger number of contacts with the oligosaccharides. PGLR has however the ability to make a larger number of contacts, which is especially relevant for salt-bridges and hydrogen-bonds (Fig. 3C). The reduced substrate dynamics when bound to histidine PGLR mutants is also reverberated into a higher number of contacts (Extended data Fig. 10). A comparison of the enzymatic motions revealed that PGLR and ADPG2, while engaged to the same decasaccharide substrate, explore separate conformational states, which are especially related to the fluctuations of unstructured regions flanking the binding groove. While for PGLR these are the regions flanking the substrate's non-reducing end (residues K108, R146, K169), in the case of ADPG2 they flank the binding cleft and in proximity of the substrate's reducing end (Extended data Fig. 11A-B). Relevant differences can also be observed between the electrostatic potentials of the two enzymes, calculated by solving the Poisson-Boltzmann equation in implicit solvent (Extended data Fig. 11C-D). Compared to ADPG2, PGLR shows a much more positively charged electrostatic potential within the substrate binding cleft, in line with pronouncedly reduced dynamics for a negatively charged (de-methylesterified) substrate, which would undergo much stronger electrostatically dominated interactions with the enzyme. Overall, subtle differences within the amino acidic composition of certain subsites can convey specifically different activity profiles from a seemingly identical fold, which is likely to generate distinct substrate binding affinities, and end-products.

PGLR and ADPG2 differ in their binding kinetics and production of OGs

The calculated RMSF shows differences in enzyme-substrate dynamics once the substrate is bound, which could reflect differences in the binding affinities of the enzymes towards specific substrates. Using fluorescence-based switchSENSE® aptasensor, we determined binding kinetics for enzyme-substrate interactions for both PGLR and ADPG2, by quantifying substrate association (k_{on}) and dissociation (k_{off}) rate constants, as well as equilibrium dissociation constant (K_D) using substrates with various degree of polymerization and methylesterification (PGA, pectins DM30%, oligogalacturonides of DP12DM5, DP12DM30, DP12DM60, Table 2). ADPG2 displayed affinities much higher for low-DM substrates (i.e. PGA and DP12DM5) than those determined with the high-DM pectins (K_D *ca.* 10 to 60 times lower; Table 2) and comparable to those of PGLR. Considering the kinetics constants, PGLR and ADPG2 show no difference for k_{on} for pectins of low DM, including PGA and DP12DM5 (1320/1120 and 953/833 $M^{-1}s^{-1}$), respectively. In contrast, when the DM of the substrate is increased (DM30%, DP12DM30 and DP12DM60), the k_{on} is always higher (~x 3 to 16 times) for PGLR compared to ADPG2. This suggest that for methylesterified pectins, PGLR, in line with the MD simulations and lower RMSF compared to ADPG2, associates much tighter with the substrate. This is as well reflected by the lower K_D determined for PGLR compared to ADPG2. No such drastic differences are measured for $k_{off,}$ as values for PGLR and ADPG2 are in the same range for most substrates.

To determine whether the differences in subsites structure, enzyme dynamics and binding affinities can translate into differences in the processivity of PGLR and ADPG2, we assessed the products generated by either of the enzymes. Using PGA as a substrate, PGLR or ADPG2 maximum activities were reached after 1-hour digestion, generating products that cannot be further hydrolysed. ADPG2 total activity was higher than that measured for PGLR. Furthermore, the addition of ADPG2 following a first hour substrate incubation with PGLR, led to an increase in total PG activity, confirming putative differences in processivity between the two enzymes, ADPG2 being able to hydrolyse PGLR's end-products (Fig. 4A). We then used a recently developed LC-MS/MS oligoprofiling approach[26] to analyse the reaction products and confirmed, using PGA as a substrate, that both enzymes have endo activities, as suggested by the structural features of the binding cleft, and that ADPG2 releases higher proportion of short-sized OGs (<DP4) compared to PGLR (Fig. 4B). On pectic substrates of DM 20-34%, the pool of OGs produced by PGLR differed to that of ADPG2 (Fig. 4C). In particular, PGLR released de-methylesterified OGs of DP5 to DP9, as well as specifically

methylesterified forms of more than 6 GalA units that were either poorly represented or absent in the pool of end-products produced by ADPG2. The main products of ADPG2 were indeed de-methylesterified OGs of DP2 to DP4, including GalA4Me (Fig. 4C, Fig. 4C, Inset). When comparing the OGs produced by PGLR, ADPG2 and AaPG1 upon enzymatic activity on pectins with DM between 20 and 34% using principal component analysis (PCA), PGLR and AaPG1 were separated according to the first dimension (Dim1 54.6.7% of the variance) while ADPG2 clustered according to second dimension (Dim2 40.4% of the variance), with main loadings being, as an example, GalA2, GalA3, GalA4Me2, GalA9Me (Extended data Fig. 12A-B). Overall, ADPG2 and PGLR have nearly identical folds that, through distinct subsite structure and enzymes' dynamics, could translate into different enzymatic processivities. Indeed, PGLR and ADPG2 differ in their intrinsic processivities, P^{Intr}, being described as the average number of consecutive catalytic acts before enzyme-substrate dissociation. P^{Intr} is dependent on the dissociation probability, P_d, calculated using the turnover number (k_{cat}) and rate constant of dissociation (k_{off})[27]. P_d values were 4.8×10^{-4} and 4.0×10^{-8}, and P^{Intr} values were 2×10^3 and 2.5×10^7, for PGLR and ADPG, respectively. This data shows that, albeit acting both as processive enzymes ($P_d << 1$), PGLR and ADPG2 differ in the extent by which they act on the substrate, with ADPG2 being much more processive than PGLR, as reflected by the lower size of the released products detected with LC-MS/MS.

The differences in PGLR and ADPG2's processivities translate into distinct effects on plant, affecting root development

Considering the localization of the expression of *PGLR* and *ADPG2* during root development, we tested the activity of both enzymes on root cell walls, whose pectins can be both methylesterified and acetylated[28]. Noticeably, PGLR released a higher proportion of acetylated OGs (including GalA5Ac, GalA6Ac, GalA6Ac2) compared to ADPG2, in addition to longer oligomers on average (Fig. 5A, Fig. 5A, Inset). Similarly, to what was observed on methylated pectins, the main OGs produced by ADPG2 were unsubstituted OGs, GalA2 and GalA3. To determine whether distinct processivities translate into distinct phenotypes, we assessed the effects of the exogenous application of purified enzymes on roots development. Iso-activities of PGLR and ADPG2 were added in the culture medium of 6-day old seedlings for either one or three days, and phenotypical changes were measured. If the application of either of the enzymes for one day did not affect root length, ADPG2 significantly impaired root elongation after three days of application (Fig. 5B). In contrast, in these conditions, PGLR had no significant effects. (Fig. 5B). To determine if the consequences of PGLR and ADPG2

application on total root length were spatially localized, we then measured the length of the firsts 50 cells from the root tip after three days of enzymes' application, using EGFP-LTI6b reporter line that specifically labels plasma membrane (Fig. 5C)[29]. Cell length was not affected by the application of either of the enzymes up to the 40th cell. In contrast, the application of ADPG2 drastically reduced the length of the cells in the elongation zone as early as cell 40; while the effects measured for PGLR were from cell 46 onwards and were lower compared to that of ADPG2 (Fig. 5D). Further differences between the enzymes can be highlighted by analysing the morphology of the root cap, the structure at the tip of the root which supports growth and protects the root meristem. The application of ADPG2 for three days had much drastic effects on root cap detachment as compared to that of PGLR suggesting that it has more drastic effects on cell-to cell adhesion (Fig. 5E). Altogether, this shows that the biochemical specificities of the two enzymes can translate into distinct effects on development.

Discussion

Polygalacturonases (PGs) enzymes play a central role in the control of pectin chemistry, contributing to changes in the cell wall mechanics, with important consequences on plant development[4–7]. In Arabidopsis, PGs are encoded by 68 genes: an abundance which is hard to rationalize within the context of the plant cell wall. Here we elucidated the structure-to-function relationships for two plant PGs, PGLR and ADPG2, whose expression overlaps in Arabidopsis roots. Both enzymes have nearly identical triple β-helix folds commonly found in other pectinases, including fungal endo-PGs[11,19,23], pectin/pectate lyases[18,30,31] and rhamnogalacturonases [17], with a large cleft opened at both sides that accommodates oligomeric substrates and confirms that PGLR and ADPG2 are endo-PGs[19]. The resolution of the crystal structure for plant PGs first rationalized the structural determinants of the absence of inhibition of plant enzymes by plant PGIPs, as PGLR activity was indeed not inhibited by *Phaseolus vulgaris* PGIP (PvPGIP2)[8]. Structurally, the key aa of *Fusarium phyllophilum* FpPG1 (S120-N121-S122-N123) needed for determining the interaction of this pathogenic PG with PvPGIP2, are absent in the T3 loop of PGLR and ADPG2. The homology modelling of Arabidopsis AtPGIP1 and AtPGIP2 further highlighted the absence of PGIP-mediated regulation of endogenous PG activity in plants as, albeit having highly conserved structure with that of PvPGIP2, they are lacking H110 and Q224 residues, required for inhibition[32]. This suggests that cellular regulation of PG is mediated by other means at the cell wall, one of which being, as demonstrated in this study, the differential processivities of the enzymes.

The main challenge in understanding subtle differences between isoforms of PGs and other carbohydrate binding enzymes (CBEs) are mostly related to the large binding interface that characterizes the interaction between CBEs and oligomeric substrates. We tackled this challenge by designing strategic mutations across the binding cleft of the structurally characterized PGLR and functionally analyzing the enzymes with combined computational and experimental methodologies. Our findings confirmed the importance of D215 for substrate hydrolysis, as well as R271 in binding and positioning the substrate at the catalytic subsite +1, as previously reported for fungal PGs[19,25]. Besides residues actively important in stabilizing the substrate, we find that other interactions in subsites flanking the catalytic subsite, crucially regulate substrate dynamics and correlate with enzymatic activity. Histidine to lysine mutants in PGLR (H196K, H237K and H196K/H237K), that might generally be important in controlling the observed pH-dependent activity of other PGs, show how the distribution of charges affects substrate dynamics. Most interestingly, substrate rigidification reported by MD upon the insertion of a positive charges across the substrate binding interface, negatively

impacts enzymatic activity as reported by the experimental biochemical characterization of the mutants. The importance of substrate dynamics in the activity of other CBEs has been also previously reported[33,34] and it might be a key factor in regulating the processive activity of CBEs more generally, with processivity being limited by substrate dissociation.

We next investigated whether the processivities of PGLR and ADPG2 differ, which could be related to their different subsite's composition affecting enzymes' dynamics. For instance, D293 and K322 in ADPG2 are replaced by T267 and A296 in PGLR, which could modify the enzyme-substrate interaction and the enzyme specificity. The determination of the dynamics, measured as the RMSF, of the enzymes in complex with a decasaccharide of GalA showed that i) for a given enzyme, the enzyme's dynamics differs with the DM of the substrate and ii) ADPG2 was overall more dynamic, with a higher RMSF, as compared to PGLR. Together with these simulations, the determination of the binding kinetics of the enzyme-substrate interactions led to hypothesizing distinct processivities for the two enzymes. When considering pectins of high DM (30%, DP12DM30, DP12DM60), the affinities of both enzymes are k_{on}-dominated, with PGLR associating much tighter with the substrate. Interestingly, the affinity of ADPG2 for the low-DM substrates is higher than that towards the high-DM pectins and is comparable to the affinities determined for PGLR. Considering the lubricating hypothesis, inferred from the studies on pectin methylesterases, and intrinsic processivity calculations, ADPG2 acts more processively on the HG chain than PGLR, and that would occur more favourably with low-DM substrates (Fig 6A-B)[33]. Altogether, these results are in accordance with the lower RMSF measured for PGLR, which would impair the sliding of the enzyme onto the chain, leading to enzyme-substrate dissociation and reiteration of enzyme attack onto the chain (Fig. 6A). Such distinct processivities effectively translated into different end-products, with ADPG2 releasing OGs of short DP (methylesterified or not) from either commercial substrates or root cell wall extracts, while PGLR released a high proportion of non-methylesterified OGs of higher DP, compared to ADPG2 (Fig. 6B). As highlighted by the fact that ADPG2 can hydrolyse PGLR-generated OGs, one could envisage a cooperative action of both enzymes in the cell wall to finely-tune HG structure during root development. A number of studies previously showed the impact of the changes in PG activity, either through the study of loss-of-function mutants or over-expressing lines in Arabidopsis, on developmental processes as diverse as dark-grown hypocotyl development, stomata formation and root development[3–8]. Our study now allows linking the enzymes' processivities to their impact on cell wall and pectins' integrity and plant development. The consequences of the exogenous application of the processive ADPG2 had indeed stronger effect on root development, including

defects in root elongation and in cell adhesion at the root cap, compared to that of PGLR. The root cap phenotype of ADPG2-treated roots is similar to that reported for *RCPG1* overexpressing lines, known to be involved in root cap removal, suggesting that enzymes might share common biochemical specificities and/or processivities[35].

Our work demonstrates that albeit having a highly conserved structural fold, subtle differences in PG structures translate into differences in enzymes' dynamics, substrate specificities, kinetics, leading to distinct processivities that play a role in the fine-tuning of plant development. This shows the extent by which, among the multigenic family, each of the isoforms has peculiar specificities that are required to control temporally and spatially pectin structure. This further highlight that, for this class of enzymes, the gene redundancy at the genome level is unlikely to reflect redundant biochemical specificities. Our study now paves the way for a better understanding of how PG's processivities can control polysaccharides chemistry and mechanical properties *in muro*.

Material and methods

Sequences retrieval and analysis

Arabidopsis thaliana PGLR (At5g14650) and ADPG2 (At2g48150) coding sequences were retrieved from publicly available genome database TAIR (https://www.arabidopsis.org/). The presence of putative signal peptide was predicted using SignalP-5.0 Server (http://www.cbs.dtu.dk/services/SignalP/). Glycosylation sites were predicted using NetNGlyc 1.0 Server (http://www.cbs.dtu.dk/services/NetNGlyc/). Sequence alignments were performed using MEGA and Clustal Omega multiple sequence alignment programs[36].

Cloning, heterologous expression and purification of PGLR and ADPG2

PGLR was previously expressed in the yeast *Pichia pastoris* and biochemically characterized[8]. PGLR mutants were created using cDNA and specific primers carrying mutations (Extended data Table 1). At2g41850 (ADPG2) coding sequence was codon-optimized for *Pichia pastoris* expression. Cloning and protein expression was done as previously described[8,37].

PGLR and ADPG2 enzyme analysis

Bradford method was used to determine the protein concentration, with bovine serum albumin (A7906, Sigma) as a standard. Deglycosylation was performed using Peptide-N-Glycosidase F (PNGase F) at 37 °C for one hour according to the supplier's protocol (New England Biolabs, Hitchin, UK). Enzyme purity and molecular weight were estimated by 12 % SDS-PAGE using

mini-PROTEAN 3 system (BioRad, Hercules, California, United States). Gels were stained using PageBlue Protein Staining Solution (Thermo Fisher Scientic) according to the manufacturer's protocol.

PGLR and ADPG2 biochemical characterization

The substrate specificity of PGLR and ADPG2 were determined with the DNS method as previously described[8,37]. Polygalacturonic acid (PGA, 81325, Sigma); Citrus pectin with DM 20-34% (P9311, Sigma), DM 55-70% (P9436, Sigma) were used as substrates. Results were expressed as nmol of GalA.min^{-1}.µg^{-1} of proteins. The optimum temperature was determined by incubating the enzymatic reaction between 25 and 60°C during 60 min using PGA (0.4%, w/v) at pH5. The pH optimum was determined between pH 4 and 7 using sodium acetate buffer (pH 3 to 5) and phosphate citrate buffer (pH 6 to 8) and 0.4 % (w/v) PGA as a substrate. The PGLR and ADPG2 kinetic parameters were calculated using GraphPad Prism8 (version 8.4.2.) with PGA as a substrate. The reactions were performed using 1 to 8 mg.ml^{-1} PGA concentrations during 10 min at 25°C in 50 mM sodium acetate (pH5). All experiments were realized in triplicate.

Digestion of cell wall pectins and released OGs profiling

OGs released after digestions by recombinant PGLR and ADPG2 were identified as described[26]. Briefly, PGA (81325, Sigma) or citrus pectin with DM 24-30% (P9311, Sigma) or OGs DP12DM5 (degree of polymerization centered on 12 and average DM of 5%) were prepared at 0.4 % (w/v) final concentration diluted in 100 mM ammonium acetate buffer (pH 5) and incubated with either PGLR and ADPG2 at 0.03 µg.µL^{-1}. Non-digested pectins were pelleted by centrifugation and the supernatant dried in speed vacuum concentrator (Concentrator plus, Eppendorf, Hamburg, Germany). The same procedure was applied for pectins from roots of Arabidopsis seedlings that were grown for 7 days at 21 °C, 16 h/8 h light/dark photoperiod. Roots were cut, incubated in ethanol 100 % (w/v) for 24 h, washed two times 5 min with acetone 100 % (w/v) and left to dry 24 h. Thirty roots per replicate were rehydrated in 150 µL 100 mM ammonium acetate pH 5 during 2 h on room temperature and digested with PGLR and ADPG2 at 0.02 µg.µL^{-1} on average, using the above-mentioned protocol. Separation of OGs was done using an ACQUITY UPLC Protein BEH SEC column (125Å, 1.7 µm, 4.6 mm x 300 mm), and the analysis was done as described[37].

Microscale thermophoresis

Molecular interactions between PGLRs (WT and mutants) and selected OGs was done using Microscale thermophoresis (MST) approach as described with some modifications[38]. Briefly, PGLRs were labelled with monolith protein labelling kit blue NHS amine reactive (Lys, NanoTemper, catalog no. MO-L003) and conserved in MST buffer (50 mM Tris pH 7.4, 150 mM NaCl, 10 mM MgCl2, 0.05 % tween-20). For all experiments, constant final concentration of labelled PGLRs was 1650 µM. Mix of OGs centred on DP12DM5 was prepared at 14028 µM concentration in MST buffer/dH_2O in 1:1 ratio. For all experiments, a constant concentration of labelled PGLRs was titrated with decreasing concentrations of non-labelled DP12DM5 from 7014 to 0.214 µM. The resulting mixtures were loaded into a Monolith NT.115 series standard capillaries (NanoTemper, catalogue no. MO-K002). Thermophoresis experiments were performed with 40% of MST power and 20% of LED power for fluorescence acquisition.

Time-resolved molecular dynamics measurements

PGLR and ADPG2 (used as ligands) were immobilized on an electro-switchable DNA biochip MPC-48-2-R1-S placed into a biosensor analyzer switchSENSE® DRX (Dynamic Biosensors GmbH, Planegg, Germany). For that, a covalent conjugate between PGLR or ADPG2 and a 48mer ssDNA was first prepared with the amine coupling kit supplied by Dynamic Biosensors and purified by anion-exchange chromatography onto a proFIRE® system (Dynamic Biosensors), then hybridized with a complementary ssDNA attached on the surface of the biochip and carrying a Cy5 fluorescent probe at its free extremity. When analytes injected in the microfluidic system bind to the oscillating dsDNA nanolevers, the nanolever movement is altered by the additional friction imposed. Kinetic measurements for 2 min (association) and for 5 min (dissociation) were performed in 5 mM sodium acetate buffer, pH 5.5, with a flow rate of 100 µl.min^{-1} at 25°C with different concentrations of various analytes: PGA (81325, Sigma), citrus pectin with DM 24-30% (P9311, Sigma) and pool of OGs centred on DP12DM5, DP12DM30 and DP12DM60 at 25, 50 and 100 µM. The fluorescence traces were analysed with the switchANALYSIS® software (V1.9.0.33, Dynamic Biosensors). The association and dissociation rates (k_{on} and k_{off}), dissociation constant ($K_D = k_{off}/k_{on}$) and the error values were derived from a global single exponential fit model, upon double referencing correction (blank and real-time)[38]. The experiments were performed in three replicates.

Intrinsic processivity calculations

The intrinsic processivity potential (P^{Intr}), a parameter corresponding to the number of consecutive catalytic steps before dissociation from the substrate was used as a measure of the processivities of PGLR and ADPG2 as described in Horn et al.[27]. The calculation of P^{Intr} is given in the Eq. 1.

$$(\text{Eq. } 1)\ P^{Intr} = -\frac{1}{\ln(1 - Pd)}$$

The dissociation probability (P_d) is expressed as a rate constant for two processes; (i) the turnover number (k_{cat}) and (ii) the enzyme–substrate complex dissociation constant (k_{off}). P_d is related to kcat and k_{off} according to Eq. 2. In the case of processive enzymes $P_d \ll 1$.

$$(\text{Eq. } 2)\ P_d = \frac{k_{off}}{k_{off} + k_{cat}}$$

The turnover number (k_{cat}) was calculated using GraphPad Prism8 (version 8.4.2.) by fitting the non-linear regression curve following the Eq. 3, where Y is enzyme velocity, X is the substrate concentration, Km is the Michaelis-Menten constant in the same units as X and Et is the concentration of enzyme catalytic sites.

$$(\text{Eq. } 3)\ \ k_{cat} = \frac{Y * (Km + X)}{Et * X}$$

Crystallization of proteins

PGLR and ADPG2 were concentrated at 10 $mg.ml^{-1}$. Crystallization was performed using the sitting-drop vapour-diffusion method. Crystallisation conditions were screened using a mosquito robot (TTP Labtech) and the PACT premier plate (Molecular dimensions, Sheffield, UK). PGLR and ADPG2 (100 nL) were mixed with an equal volume of precipitant (1:1). The crystals that resulted in best diffraction data were obtained with 0.2 M sodium fluoride, 0.1 M bis-tris propane pH 8.5, 20 % w/v PEG 3350 (H1 condition, PACT premier plate) for PGLR and 0.2 M sodium malonate dibasic monohydrate, 20 % w/v PEG 3350 (E12 condition, PACT premier plate) for ADPG2. Crystals for PGLR and ADPG2 formed after 6 and 2 months, respectively. Scale-up of the best condition was realized by mixing 1 µl of the best precipitant condition with 1 µl of the enzyme in the hanging drop vapor-diffusion method.

X-ray data collection and processing

Crystals were mixed with precipitation solution and PEG 3350 (35% w/v) before mounting in a loop and flash cooling in liquid nitrogen. The diffraction data were collected at PROXIMA-1 beamline (Synchrotron Soleil, Saint Aubin, France), at a temperature of -173°C using a PILATUS 6M end EIGER 16M detector (Dectris). Data were collected using X-rays with wavelength of 0. 978564 Å. For PGLR, three data sets were collected from the same crystal at 1.3 Å resolution. Intensities were integrated, scaled and merged using XDS[39] and XSCALE[40]. For ADPG2, one data set was collected at 2.03 Å resolution. Intensities were processed using XDS[39]. PGLR crystal belonged to triclinic space group P1 with one molecule in asymmetric unit, while ADPG2 belongs to orthorhombic space group $P2_12_12_1$ with two molecules in asymmetric units.

Structure solution and refinement and analysis

For PGLR and ADPG2 structure and function prediction I-TASSER prediction software was used[41]. ColabFold was used for AtPGIP1 and AtPGIP2 models[42]. The structure of PGLR was solved by molecular replacement using *Phaser*[43]. The data were phased using rhamnogalacturonase A (PDB: 1RMG, Uniprot: Q00001) as a search model[17]. Model was built using *Autobuild* and refined using *Refine* from PHENIX suite[44]. The model was iteratively improved with *Coot*[45] and *Refine*. ADPG2 structure was solved by molecular replacement using PGLR as a starting model and the above-mentioned iterative procedure. The final structure for PGLR and ADPG2 have been deposited in the Protein Data Bank as entries 7B7A and 7B8B, respectively. UCSF Chimera was used for creation of graphics[46].

Modelling and molecular dynamics simulations

Molecular dynamics (MD) simulations were carried out on both the WT PGLR and ADPG2 proteins in complex with fully de-methylesterified polygalacturonate decasaccharides, as well as partially methylesterified polygalacturonate decasaccharides. Additionally, PGLR mutants H196K and H237K, modelled from the resolved X-ray crystal structures using PyMOL, were also simulated, in complex with fully de-methylesterified polygalacturonate decasaccharides [47]. Molecular topologies of the complexes were created according to the parameters of the AMBER14SB_parmbsc1 forcefield[48]. The complexes were placed in cubic boxes with a solute-box distance of 1.0 nm and solvated with water molecules parameterised according to the TIP3P water model[49]. To neutralise the system's net charge and reach a salt concentration of 0.165 M, Na^+ and Cl^- ions were added before energy-minimisation was performed.

The systems were then energy minimized, to resolve clashes between particles using a steep-descent algorithm with a step size of 0.01, considering convergence when the particle-particle force was 1000 kJ mol^{-1} nm^{-1}. Particle-particle forces were computing considering van der Waals and electrostatic interactions occurring up to 1.0 nm, treating long-range electrostatics in the Fourier space using the Particle Mesh Ewald (PME) summation method.

After minimization, solvent equilibration was achieved in two stages to reach constant temperature and pressure. The first stage was performed in the nVT ensemble while the second in the nPT ensemble. Solvent equilibration through the nVT ensemble was carried out for 1 ns, with the equation of motion integrated with a time step of 2 fs, targeting a reference temperature of 310.15 K coupled every 0.1 ps using the V-rescale thermostat[50].

In this step, each particle in the system was assigned random velocities based on the Maxwell-Boltzmann distribution[51] obtained at 310.15 K. Equilibration of the solvent through the nPT ensemble was then carried out for 1 ns starting from the last step (coordinates and velocities) of the previous equilibration, at a reference temperature of 310.15 K, coupled every 0.1 ps using the V-rescale thermostat[50]. In this step, pressure coupling was conducted at 1 bar, with pressure coupled isotropically every 2.0 ps using the Parrinello-Rahman barostat[52]. Particle-particle interactions were calculated by building pair lists using the Verlet scheme. A cutoff of 1.0 nm was used to compute short-range van der Waals and electrostatic interactions sampled via a Coulomb potential. The Particle Mesh Ewald (PME) algorithm[53], with a Fourier grid spacing of 0.16 and a cubic B-spline interpolation level of 4, was used to compute, in the Fourier space, long-range electrostatic interactions past the cutoff.

Simulations were then performed on both in-house machines and on NeSI's (New Zealand eScience Infrastructure) high performance cluster, Mahuika, using GROMACS (Groningen MAchine for Chemical Simulation) version 2020.5[54]. For each of the 6 complexes, simulations were run for 200 ns using a time step of 2 fs and replicated 5 times for a total simulation time of 1 μs per complex. Each replicate differed in terms of the random sets of particle velocities generated through the nVT ensemble. Molecular dynamics trajectories were recorded every 10 ps. For analysis, the first 50 ns of each production run were considered equilibration time and discarded.

Analyses were conducted using in-house Python 3 scripts implemented Jupyter notebooks[55]. Porcupine plots were created using data from a normalised principal component analysis calculated using GROMACS. Figures were created and rendered with Matplotlib[56], VMD (Visual Molecular Dynamics)[57] and UCSF Chimera[46].

Poisson-Boltzmann calculations of electrostatic potentials

The protonation states of each amino acid were assigned according to the pKa curves calculated at pH = 4 for PGLR and pH = 5 for ADPG2, using the PROPKA software[58]. Atomic charges and radii for the protein atoms were assigned using the PDB2PQR software[59] according to the parameters of the AMBER14SB_parmbsc1 forcefield[48], while atomic charges and radii for the sugar atoms were obtained from our previous work[60]. The surface electrostatic potentials for WT PGLR and ADPG2 were then calculated solving the non-linearized form of the Poisson-Boltzmann equation through the APBS (Adaptive Poisson–Boltzmann Solver) software on a cubic grid composed of 193 grid points across the x-, y- and z- directions[61]. These calculations followed a stepwise approach where the Poisson-Boltzmann equation is first solved on a coarse mesh grid with a length of 155 Å and a spacing of 0.8 Å; then on a fine mesh grid with a length of 125 Å and a spacing of 0.64 Å. Calculations were solved considering a temperature of 218.15 K with a mobile ionic charge of +/- 1 e_c, an ionic concentration of 0.165 M and an ionic radius of 2.0 Å. The protein dielectric constant was set at 4.0 and the solvent dielectric constant was set to 78.54. The protein surface electrostatic potentials were then visualised and coloured on the protein's molecular surface using VMD[57].

Exogenous application of enzymes on Arabidopsis seedlings

20-30 sterile seeds of Arabidopsis thaliana EGFP-LTI6b[29] plasma membrane marker-lines were sowed in 400 µL liquid Arabidopsis Murashige and Skoog medium (Sucrose, MES (Duchefa monohydrate), MS commerciale in 24 well-plates [62]. After 48 hours stratification, plates were placed in growth chamber under long day conditions (16 hours photoperiod, 120µmoles/m²/s, 21°C). After 6 days, cultures were supplemented with 0.051 µg/µL and 0.015 µg/µ filter-sterilized PGLR and ADPG2, respectively using 0.2 µm PES filter (Whatman TM Puradisc TM 13 mm) in a volume of liquid MS medium of 200 µL to reach iso-activity. Plantlets were allowed to grown for another 1 day (T1) or 3 days (T3). Negative controls correspond to 6-, 7- or 9-days cultures without enzyme (T0 ØEnz, T1 ØEnz and T3 ØEnz, respectively). For each of these conditions, measurements of primary root lengths were done using ImageJ software with NeuronJ plugin. For each condition, 30-40 plants were measured. For cell lengths determination, approximately 1 mm from the tip of the root of 3 to 7 plants were photographed under a steromicroscope (ZEISS SteREO Discovery.V20). Images were assembled using MosaicJ plugin from Image J. The length of the firsts 50 epidermal cells, starting from the first cell of the columella, were measured using image J software with NeuronJ plugin. Phenotypical

593 observations where performed following ruthenium red staining (0.05 % (w/v) in water, Sigma-
594 Aldrich R-2751) under binocular microscope (Leica EZ4).

595

Acknowledgements

This work was supported by a grant from the Agence Nationale de la Recherche (ANR-17-CE20-0023) and by the Conseil Regional Hauts-de-France and the FEDER (Fonds Européen de Développement Régional) through a PhD studentship awarded for to J.S. We wish to thank Pierre Legrand and all the staff at Proxima1 beamline (Synchrotron SOLEIL, Gif sur Yvette, France) for X-ray diffraction and data collection. The technical assistance of Maša Boras, a former master student is gratefully acknowledged.

Author's contribution

J.P., F.S., V.L. and D.M. designed research; J.S., W.T., V.U., A.L., O.H.; J.B., A.V., S.B., M.R., P.P., E.B., S.P., D.S.L, M.M.R., J-M.G., D.M., C. P-R., and V.L. performed research; J.S., W.T., V.U., A.L., R.M., J-X.F., J-M.G., D.M., V.L., F.S. and J.P. analyzed data; J.S., W.T., F.S., V.L., D.M., and J.P. wrote the paper with input from J.B., E.B., J-M.G, M.M.R.

Conflicts of interest

There are no conflicts of interest.

Literature

1. Bidhendi, A. J. & Geitmann, A. Relating the mechanics of the primary plant cell wall to morphogenesis. *J. Exp. Bot.* **67**, 449–461 (2016).

2. Mohnen, D. Pectin structure and biosynthesis. *Curr. Opin. Plant Biol.* **11**, 266–277 (2008).

3. Rhee, S. Y., Osborne, E., Poindexter, P. D. & Somerville, C. R. Microspore Separation in the quartet 3 Mutants of Arabidopsis Is Impaired by a Defect in a Developmentally Regulated Polygalacturonase Required for Pollen Mother Cell Wall Degradation. *Plant Physiol.* **133**, 1170–1180 (2003).

4. Ogawa, M., Kay, P., Wilson, S. & Swain, S. M. Arabidopsis Dehiscence Zone Polygalacturonase1 (ADPG1), ADPG2, and Quartet2 are polygalacturonases required for cell separation during reproductive development in Arabidopsis. *Plant Cell* **21**, 216–233 (2009).

5. Xiao, C., Somerville, C. & Anderson, C. T. POLYGALACTURONASE INVOLVED IN EXPANSION1 functions in cell elongation and flower development in Arabidopsis. *Plant Cell* **26**, 1018–1035 (2014).

6. Xiao, C. *et al.* Activation tagging of Arabidopsis POLYGALACTURONASE INVOLVED IN EXPANSION2 promotes hypocotyl elongation, leaf expansion, stem lignification, mechanical stiffening, and lodging. *Plant J.* **89**, 1159–1173 (2017).

7. Rui, Y. *et al.* POLYGALACTURONASE INVOLVED IN EXPANSION3 functions in seedling development, rosette growth, and stomatal dynamics in Arabidopsis thaliana. *Plant Cell* **29**, 2413–2432 (2017).

8. Hocq, L. *et al.* The exogenous application of AtPGLR, an endo -polygalacturonase, triggers pollen tube burst and repair. *Plant J.* **103**, 617–633 (2020).

9. Mutuku, J. M., Cui, S., Yoshida, S. & Shirasu, K. Orobanchaceae parasite–host interactions. *New Phytol.* **230**, 46–59 (2021).

10. Markovič, O. & Janeček, Š. Pectin degrading glycoside hydrolases of family 28: sequence-structural features, specificities and evolution. *Protein Eng. Des. Sel.* **14**, 615–631 (2001).

652 11. Cho, S. W., Lee, S. & Shin, W. The X-ray structure of Aspergillus aculeatus
653 Polygalacturonase and a Modeled structure of the Polygalacturonase-Octagalacturonate
654 Complex. *J. Mol. Biol.* **311**, 863–878 (2001).

655 12. Abbott, D. W. & Boraston, A. B. The Structural Basis for Exopolygalacturonase
656 Activity in a Family 28 Glycoside Hydrolase. *J. Mol. Biol.* **368**, 1215–1222 (2007).

657 13. Benedetti, M. *et al.* Structural resolution of the complex between a fungal
658 polygalacturonase and a plant polygalacturonase-inhibiting protein by small-angle x-
659 ray scattering. *Plant Physiol.* **157**, 599–607 (2011).

660 14. Ferrari, S. *et al.* Oligogalacturonides: plant damage-associated molecular patterns and
661 regulators of growth and development. *Front. Plant Sci.* **4**, 1–9 (2013).

662 15. Davidsson, P. *et al.* Short oligogalacturonides induce pathogen resistance-associated
663 gene expression in Arabidopsis thaliana. *BMC Plant Biol.* **17**, 1–17 (2017).

664 16. González-Carranza, Z. H., Elliott, K. A. & Roberts, J. A. Expression of
665 polygalacturonases and evidence to support their role during cell separation processes
666 in Arabidopsis thaliana. *J. Exp. Bot.* **58**, 3719–3730 (2007).

667 17. Petersen, T. N., Kauppinen, S. & Larsen, S. The crystal structure of
668 rhamnogalacturonase a from Aspergillus aculeatus: A right-handed parallel β helix.
669 *Structure* **5**, 533–544 (1997).

670 18. Yoder, M. D. & Jurnak, F. The Refined Three-Dimensional Structure of Pectate Lyase
671 C lmplications for an Enzymatic Mechanism. *Plant Physiol* **107**, 349–364 (1995).

672 19. van Santen, Y. *et al.* 1.68-angstrom crystal structure of endopolygalacturonase II from
673 Aspergillus niger and identification of active site residues by site-directed mutagenesis.
674 *J. Biol. Chem.* **274**, 30474–30480 (1999).

675 20. Benedetti, M. *et al.* A single amino-acid substitution allows endo-polygalacturonase of
676 Fusarium verticillioides to acquire recognition by PGIP2 from Phaseolus vulgaris.
677 *PLoS One* **8**, 1–11 (2013).

678 21. Federici, L. *et al.* Structural requirements of endopolygalacturonase for the interaction
679 with PGIP (polygalacturonase-inhibiting protein). *Proc. Natl. Acad. Sci. U. S. A.* **98**,
680 13425–13430 (2001).

681 22. André-Leroux, G., Tessier, D. & Bonnin, E. Endopolygalacturonases reveal molecular
682 features for processivity pattern and tolerance towards acetylated pectin. *Biochim.*
683 *Biophys. Acta - Proteins Proteomics* **1794**, 5–13 (2009).

684 23. Shimizu, T., Nakatsu, T., Miyairi, K., Okuno, T. & Kato, H. Active-site architecture of
685 endopolygalacturonase I from Stereum purpureum revealed by crystal structures in
686 native and ligand-bound forms at atomic resolution. *Biochemistry* **41**, 6651–6659
687 (2002).

688 24. Pagès, S., Heijne, W. H. M., Kester, H. C. M., Visser, J. & Benen, J. A. E. Subsite
689 mapping of Aspergillus niger endopolygalacturonase II by site-directed mutagenesis. *J.*
690 *Biol. Chem.* **275**, 29348–29353 (2000).

691 25. Park, K.-C., Kwon, S.-J., Kim, P.-H., Bureau, T. & Kim, N.-S. Gene structure
692 dynamics and divergence of the polygalacturonase gene family of plants and fungus.
693 *Genome* **51**, 30–40 (2008).

694 26. Voxeur, A. *et al.* Oligogalacturonide production upon Arabidopsis thaliana-Botrytis
695 cinerea interaction. *Proc. Natl. Acad. Sci. U. S. A.* **116**, 19743–19752 (2019).

696 27. Horn, S. J., Sorlie, M., Vårum, K. M., Väljamäe, P. & Eijsink, V. G. H. Measuring
697 processivity. *Methods Enzymol.* **510**, 69–95 (2012).

698 28. Willats, W. G. T., McCartney, L., Mackie, W. & Knox, J. P. Pectin: cell biology and
699 prospects for functional analysis. *Plant Mol. Biol.* **47**, 9–27 (2001).

700 29. Kurup, S. *et al.* Marking cell lineages in living tissues. *Plant J.* **42**, 444–453 (2005).

701 30. Vitali, J., Schick, B., Kester, H. C. M., Visser, J. & Jurnak, F. The Three-Dimensional
702 Structure of Aspergillus niger Pectin Lyase B at 1.7-Å Resolution. *Plant Physiol.* **116**,
703 69–80 (1998).

704 31. Lietzke, S. E., Scavetta, R. D., Yoder, M. D. & Jurnak, F. The Refined Three-
705 Dimensional Structure of Pectate Lyase E from Erwinia chrysanthemi at 2.2 A
706 Resolution. *Plant Physiol.* **111**, 73–92 (1996).

707 32. Ferrari, S., Vairo, D., Ausubel, F. M., Cervone, F. & De Lorenzo, G. Tandemly
708 duplicated Arabidopsis genes that encode polygalacturonase-inhibiting proteins are
709 regulated coordinately by different signal transduction pathways in response to fungal
710 infection. *Plant Cell* **15**, 93–106 (2003).

711 33. Mercadante, D., Melton, L. D., Jameson, G. B., Williams, M. A. K. & De Simone, A.
712 Substrate dynamics in enzyme action: Rotations of monosaccharide subunits in the
713 binding groove are essential for pectin methylesterase processivity. *Biophys. J.* **104**,
714 1731–1739 (2013).

715 34. Mercadante, D., Melton, L. D., Jameson, G. B. & Williams, M. A. K. Processive pectin
716 methylesterases: The role of electrostatic potential, breathing motions and bond
717 cleavage in the rectification of brownian motions. *PLoS One* **9**, 1–11 (2014).

718 35. Kamiya, M. *et al.* Control of root cap maturation and cell detachment by BEARSKIN
719 transcription factors in Arabidopsis. *Development* **143**, 4063–4072 (2016).

720 36. Kumar, S., Stecher, G., Li, M., Knyaz, C. & Tamura, K. MEGA X: Molecular
721 Evolutionary Genetics Analysis across Computing Platforms. *Mol. Biol. Evol.* **35**,
722 1547–1549 (2018).

723 37. Safran, J. *et al.* New insights into the specificity and processivity of two novel
724 pectinases from Verticillium dahliae. *Int. J. Biol. Macromol.* **176**, 165–176 (2021).

725 38. Sénéchal, F. *et al.* Structural and dynamical characterization of the pH-dependence of
726 the pectin methylesterase-pectin methylesterase inhibitor complex. *J. Biol. Chem.* **292**,
727 21538–21547 (2017).

728 39. Kabsch, W. Integration, scaling, space-group assignment and post-refinement. *Acta*
729 *Crystallogr. Sect. D Biol. Crystallogr.* **66**, 133–144 (2010).

730 40. Kabsch, W. Xds. *Acta Crystallogr. D. Biol. Crystallogr.* **66**, 125–32 (2010).

731 41. Zhang, Y. I-TASSER server for protein 3D structure prediction. *BMC Bioinformatics*
732 **9**, 1–8 (2008).

733 42. Mirdita, M. *et al.* ColabFold - Making protein folding accessible to all. *bioRxiv*
734 2021.08.15.456425 (2022).

735 43. McCoy, A. J. *et al.* Phaser crystallographic software. *J. Appl. Crystallogr.* **40**, 658–674
736 (2007).

737 44. Liebschner, D. *et al.* Macromolecular structure determination using X-rays, neutrons
738 and electrons: Recent developments in Phenix. *Acta Crystallogr. Sect. D Struct. Biol.*
739 **75**, 861–877 (2019).

45. Emsley, P., Lohkamp, B., Scott, W. G. & Cowtan, K. Features and development of Coot. *Acta Crystallogr. Sect. D Biol. Crystallogr.* **66**, 486–501 (2010).

46. Pettersen, E. F. *et al.* UCSF Chimera--A visualization system for exploratory research and analysis. *J. Comput. Chem.* **25**, 1605–1612 (2004).

47. The PyMOL Molecular Graphics System. Version 2.0 Schrödinger, LLC.

48. Lindorff-Larsen, K. *et al.* Improved side-chain torsion potentials for the Amber ff99SB protein force field. *Proteins Struct. Funct. Bioinforma.* **78**, 1950–1958 (2010).

49. Jorgensen, W. L., Chandrasekhar, J., Madura, J. D., Impey, R. W. & Klein, M. L. Comparison of simple potential functions for simulating liquid water. *J. Chem. Phys.* **79**, 926–935 (1983).

50. Berendsen, H. J. C., Postma, J. P. M., Van Gunsteren, W. F., Dinola, A. & Haak, J. R. Molecular dynamics with coupling to an external bath. *J. Chem. Phys.* **81**, 3684–3690 (1984).

51. Rowlinson, J. S. The Maxwell-boltzmann distribution. *Mol. Phys.* **103**, 2821–2828 (2005).

52. Parrinello, M. & Rahman, A. Polymorphic transitions in single crystals: A new molecular dynamics method. *J. Appl. Phys.* **52**, 7182–7190 (1981).

53. Darden, T., York, D. & Pedersen, L. Particle mesh Ewald: An N·log(N) method for Ewald sums in large systems. *J. Chem. Phys.* **98**, 10089–10092 (1993).

54. Van Der Spoel, D. *et al.* GROMACS: Fast, flexible, and free. *J. Comput. Chem.* **26**, 1701–1718 (2005).

55. Kluyver, T. *et al.* Jupyter Notebooks—a publishing format for reproducible computational workflows. *Position. Power Acad. Publ. Play. Agents Agendas - Proc. 20th Int. Conf. Electron. Publ. ELPUB 2016* 87–90 (2016) doi:10.3233/978-1-61499-649-1-87.

56. Hunter, J. D. Matplotlib: A 2D graphics environment. *Comput. Sci. Eng.* **9**, 90–95 (2007).

57. Humphrey, W., Dalke, A. & Schulten, K. VMD: Visual Molecular Dynamics. *J. Mol. Graph.* **14**, 33–38 (1996).

58. Søndergaard, C. R., Olsson, M. H. M., Rostkowski, M. & Jensen, J. H. Improved treatment of ligands and coupling effects in empirical calculation and rationalization of p K a values. *J. Chem. Theory Comput.* **7**, 2284–2295 (2011).

59. Dolinsky, T. J., Nielsen, J. E., McCammon, J. A. & Baker, N. A. PDB2PQR: An automated pipeline for the setup of Poisson-Boltzmann electrostatics calculations. *Nucleic Acids Res.* **32**, 665–667 (2004).

60. Irani, A. H., Mercadante, D. & Williams, M. A. K. On the electrophoretic mobilities of partially charged oligosaccharides as a function of charge patterning and degree of polymerization. *Electrophoresis* **39**, 1497–1503 (2018).

61. Jurrus, E. *et al.* Improvements to the APBS biomolecular solvation software suite. *Protein Sci.* **27**, 112–128 (2018).

62. Murashige, T. & Skoog, F. A Revised Medium for Rapid Growth and Bio Assays with Tobacco Tissue Cultures. *Physiol. Plant.* **15**, 473–497 (1962).

Characteristics	PGLR	ADPG2
Data collection		
Diffraction source	PROXIMA1A	PROXIMA1A
Wavelength (Å)	0.978	0. 978
Temperature (°C)	100.15	100.15
Detector	PILATUS3 6M	EIGER 16M
Crystal to detector distance (mm)	190.0	279.3
Rotation range per image (°)	0.1	0.1
Total rotation range (°)	360	360
Crystal data		
Space group	P1	$P\ 2_12_12_1$
a, b, c (Å)	38.97, 41.83, 63.33	71.78, 88.56, 113.87
α, β, γ, (°)	93.25, 99.86, 114.95	90.00, 90.00, 90.00
Subunits per asymmetric unit	1	2
Data statistics		
Resolution range (Å)	33.33 - 1.3	44.61 - 2.03
Total No. of reflection	761821 (55201)	645204 (65696))
No. of unique reflection	83668 (8043)	47381 (4654)
No. of reflections, test set	4182 (401)	2368 (233)
R_{merge} (%)	7.64 (77.7)	8.9 (97)
Completeness (%)	96.1 (92.0)	99.9 (99.3)
($I/\sigma(I)$)	16.24 (2.78)	16.91 (2.56)
Multiplicity	9.1(6.9)	13.6 (14.0)
$CC_{1/2}$ (%)	99 (86.3)	99 (92.1)
Refinement		
R_{crys} /R_{free} (%)	14. 2 / 17.7	18.9 / 23.0
Average B - factor (Å^2)	29.1	27.89
No. of non-H atoms		
Protein	3085	5563
Ion	-	5
Ligand	100	-
Water	609	999
Total	3794	6567
R.m.s. deviations		
Bonds (Å)	0.015	0.006
Angles (°)	1.59	1.06
Ramachandran plot		
Most favoured (%)	94.6	93.58
Allowed (%)	5.4	6.28
Outlier (%)	-	0.14

Table 1. Data collection, processing and refinement statistics for PGLR and ADPG2. Statistics for the highest-resolution shell are shown in parentheses.

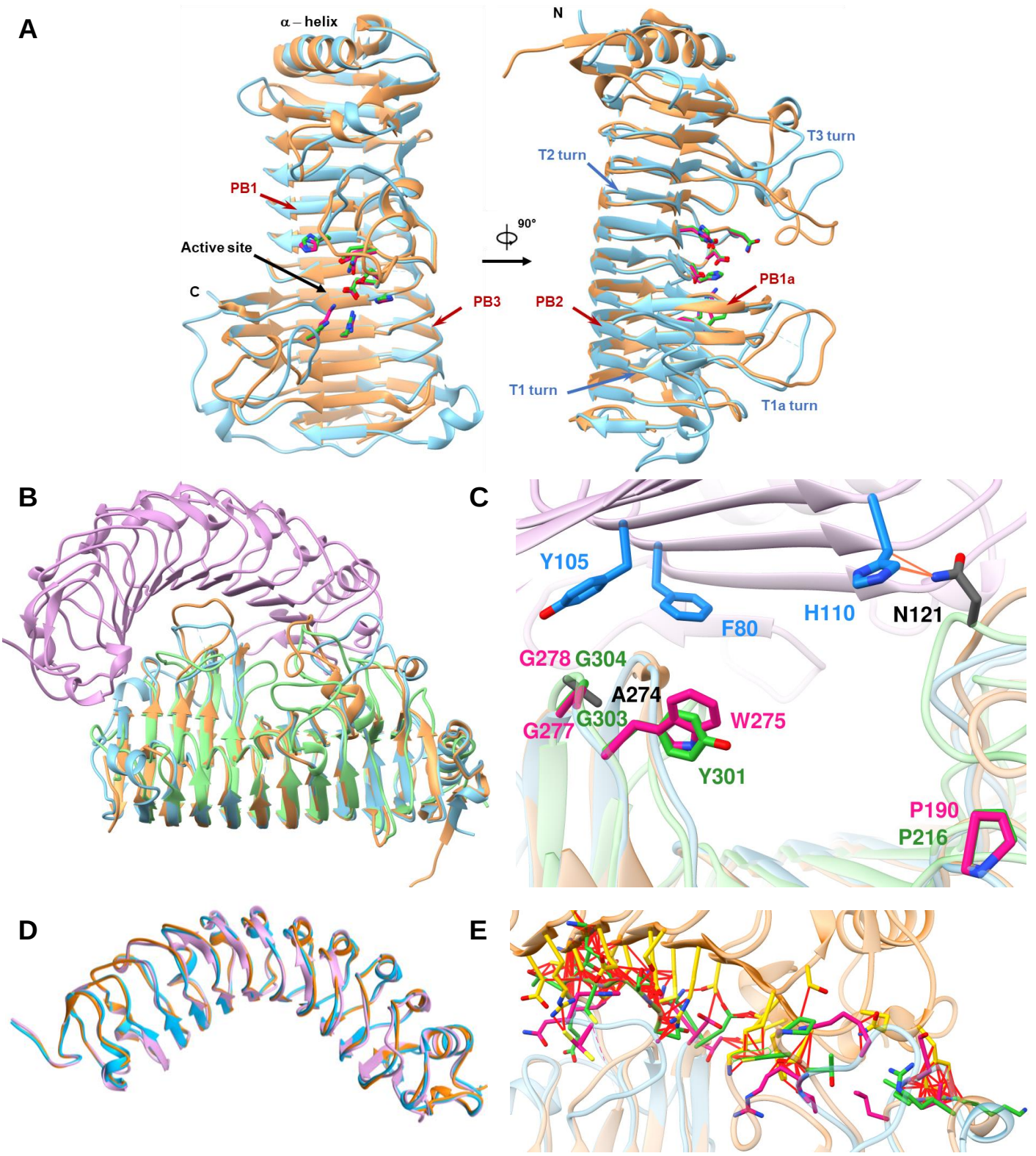

Fig 1. Structure comparison of PGLR and ADPG2 and identification of novel amino-acids required for activity
A) Overall structure of PGLR and ADPG2 represented in ribbon diagrams which are colored in blue and brown, respectively. Right-handed parallel β-helical structure consisting of β-strands (red) and turns (blue). PGLR and ADPG2 active site amino acids are pink and green colored. β-sheets are turns are indicated by red and blue arrows. B) Ribbon representation of *Phaseolus vulgaris* PGIP2 (PvPGIP2, plum), PGLR (blue), ADPG2 (brown), *Fusarium phyllophilum* PG (FpPG1, green). C) Detailed representation of aa involved in PvPGIP2-FpPG1 interaction (PvPGIP2 amino-acids in blue and FpPG1 amino-acids in grey), with orange lines representing van der Waals contacts. Key aa (N121, A274) mediating the interaction in FpPG1 are absent in PGLR and ADPG2. D) Superimposition of crystallised PvPGIP2 with models of Arabidopsis PGIP1 (AtPGIP1,orange) and PGIP2 (AtPGIP2, blue). E) Interactions of AtPGIP1 with PGLR and ADPG2. Amino acids of AtPGIP1 (yellow), PGLR (pink) and ADPG2 (green) included in clashes closer than 0.6 Å are shown .The red lines represent atoms overlap of minimum 0.6 Å.

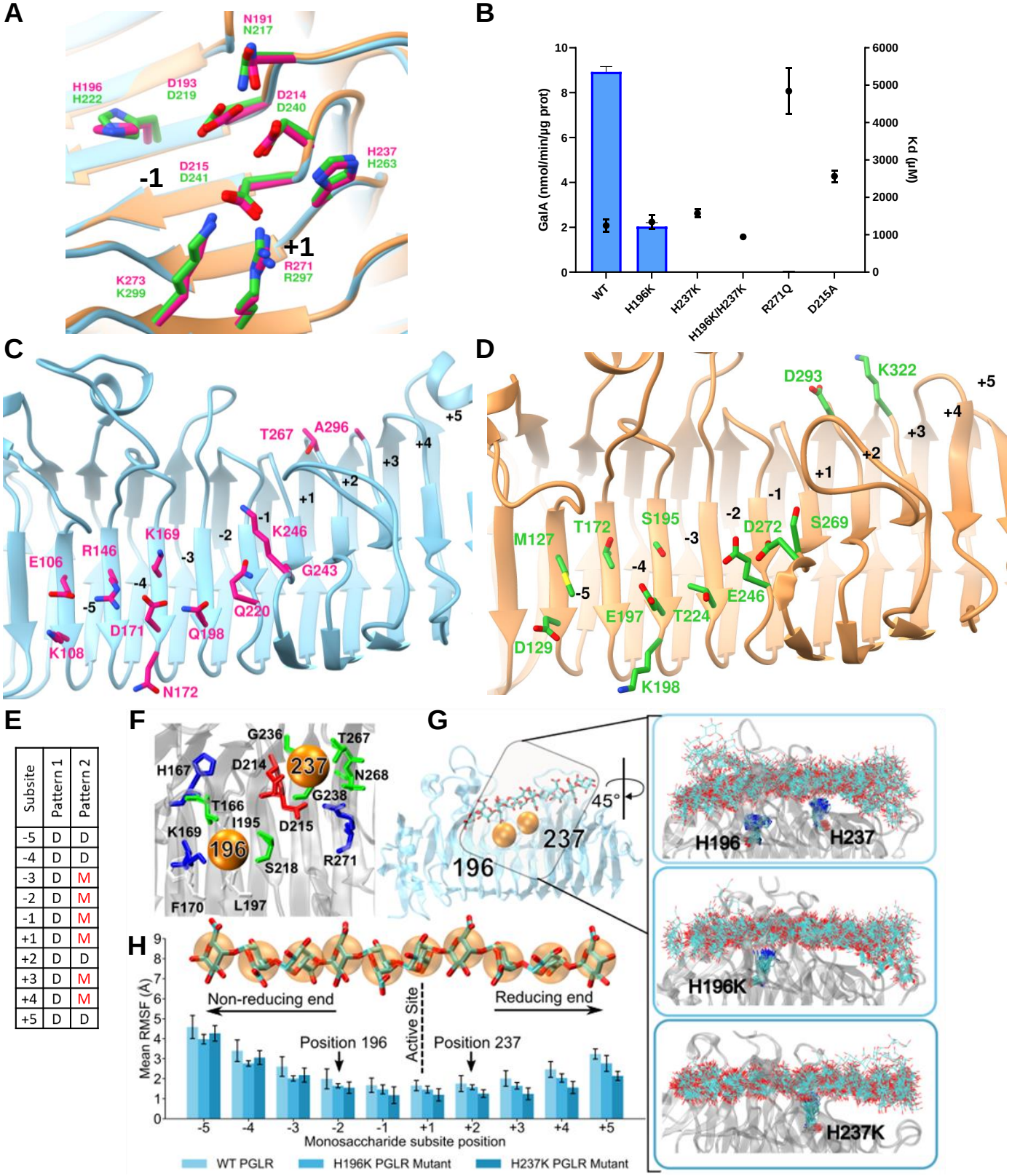

Subsite	Pattern 1	Pattern 2
-5	D	D
-4	D	D
-3	D	M
-2	D	M
-1	D	M
+1	D	M
+2	D	D
+3	D	M
+4	D	M
+5	D	D

Figure 2: Structure of the PGLR-ADPG2 active site and binding groove. Role of H196 and 237 for PG activity
A) Active site of the PGLR and ADPG2 highlighting absolutely conserved aa. D193, D214 and D215 are aa involved in substrate hydrolysis. Black numbers indicate the subsites. B) Total PG activity of WT and mutated forms of PGLR (H196K, H237K, H196K/H237K, R271Q, D217A) on PGA (blue bars) and MST analysis of the interaction between WT and mutated forms of PGLR using a substrate of DP12 and DM5 (black dots). C) Structure of PGLR binding groove (subsite -5 to +5). D) Structure of ADPG2 binding grove (subsites -5 to +5). E) Sequence of the fully de-methylesterified (pattern 1) or 60% methylesterified (pattern 2) decasaccharides simulated in complex with ADPG2 and PGLR. D: de-methylesterified GalA, M: methylesterified GalA. F) cross-section of the substrate binding groove highlighting the positions of H196 and H237, which are represented as orange spheres. Positively and negatively charged residues are shown in blue and red, respectively, while polar residues are shown in green and represented as sticks. G) PGLR in complex with a decasaccharides substrate, in the insets the conformational ensembles of the substrate and of H196, H237 and H196/H237 are shown, by reporting conformations obtained every 10 ns. H) Root mean square fluctuations (RMSF) of each monosaccharide across the binding groove for WT PGLR and its mutants.

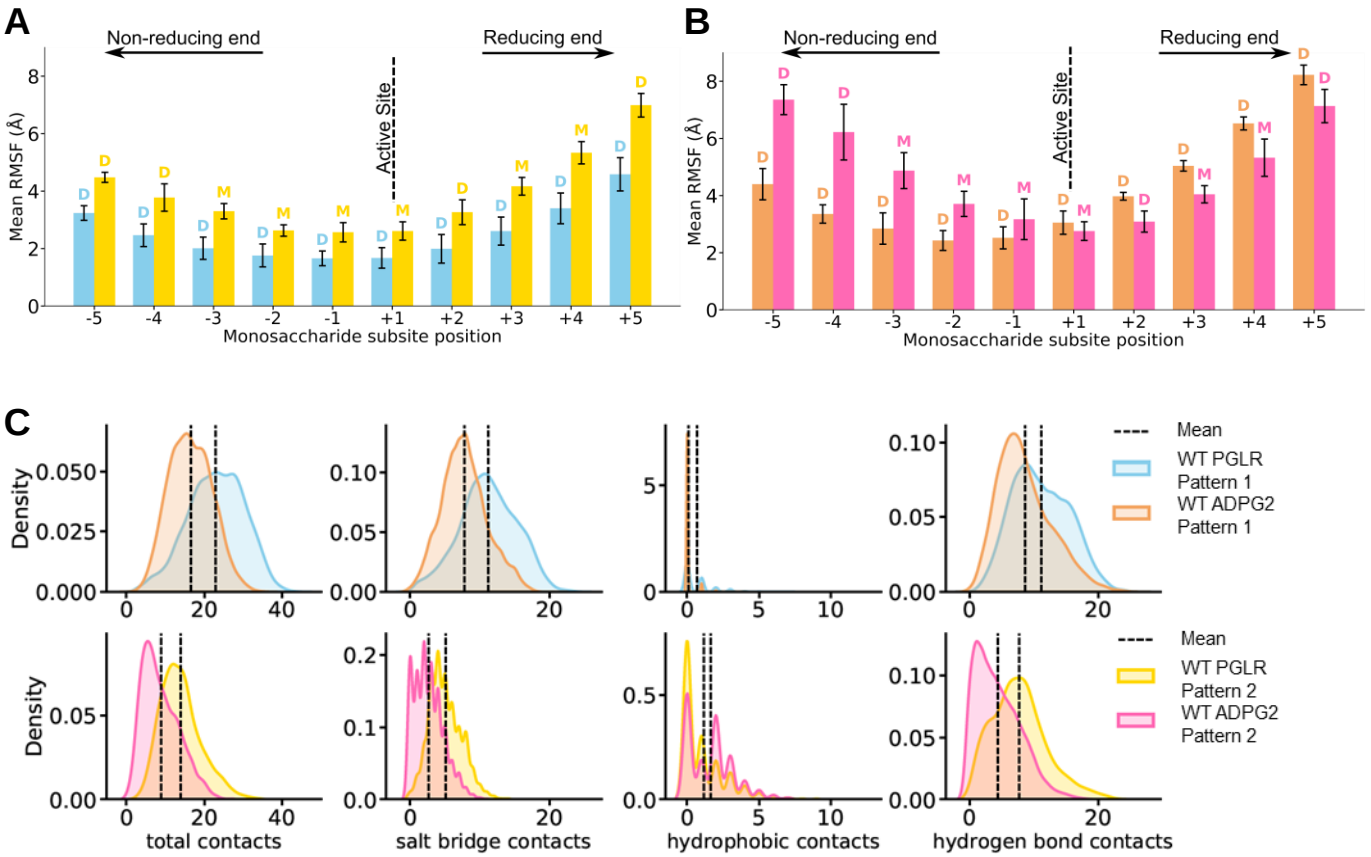

Fig 3. PGLR and ADPG2 show distinct substrate dynamics.
A-B) Root mean square fluctuations (RMSF) of each monosaccharide bound across the binding groove of PGLR (A) or ADPG2 (B). In each panel, fully de-methylesterified (pattern 1 – cyan in A and orange in B) or 60% methylesterified decasaccharides (pattern 2 – yellow in A and pink in B) are shown. C) Analysis of the contacts between PGLR or ADPG2 and substrates either fully de-methylesterified (pattern 1) or characterized by 60% methylesterification (pattern 2).

	PGLR						ADPG2					
	K_D (µM)		k_{on} ($M^{-1}s^{-1}$)		k_{off} (ms^{-1})		K_D (µM)		k_{on} ($M^{-1}s^{-1}$)		k_{off} (ms^{-1})	
Substrate	**mean**	**SD**	**mean**	**SD**	**mean**	**SD**	**mean**	**SD**	**mean**	**SD**	**mean**	**SD**
PGA	8.12	0.68	1320	110	10.7	0.2	4.3	1.1	1120	230	4.8	0.8
DM30	12.1	2.2	1010	180	12.2	0.4	194	89	62.8	28.6	12.2	0.3
DP12DM5	12.6	1	953	71	12	0.3	10.7	0.9	833	64	8.9	0.3
DP12DM30	26.8	3.6	268	23	7.2	0.7	267	79	28.8	7.8	7.7	0.9
DP12DM60	38	7.4	196	29	7.5	0.9	155	47	54.9	16.0	8.5	0.7

Table 2. k_{on}, k_{off} and k_D measurements for PGLR and ADPG using substrates of various degrees of polymerization. PGA: Polygalacturonic acid, DM30: Commercial pectins of DM30%, DP12DM5/DP12DM30/DP12DM60: Pool of OG centered on DP12 with increasing DM (5%, 30%, 60%). Data shown average of three replicates.

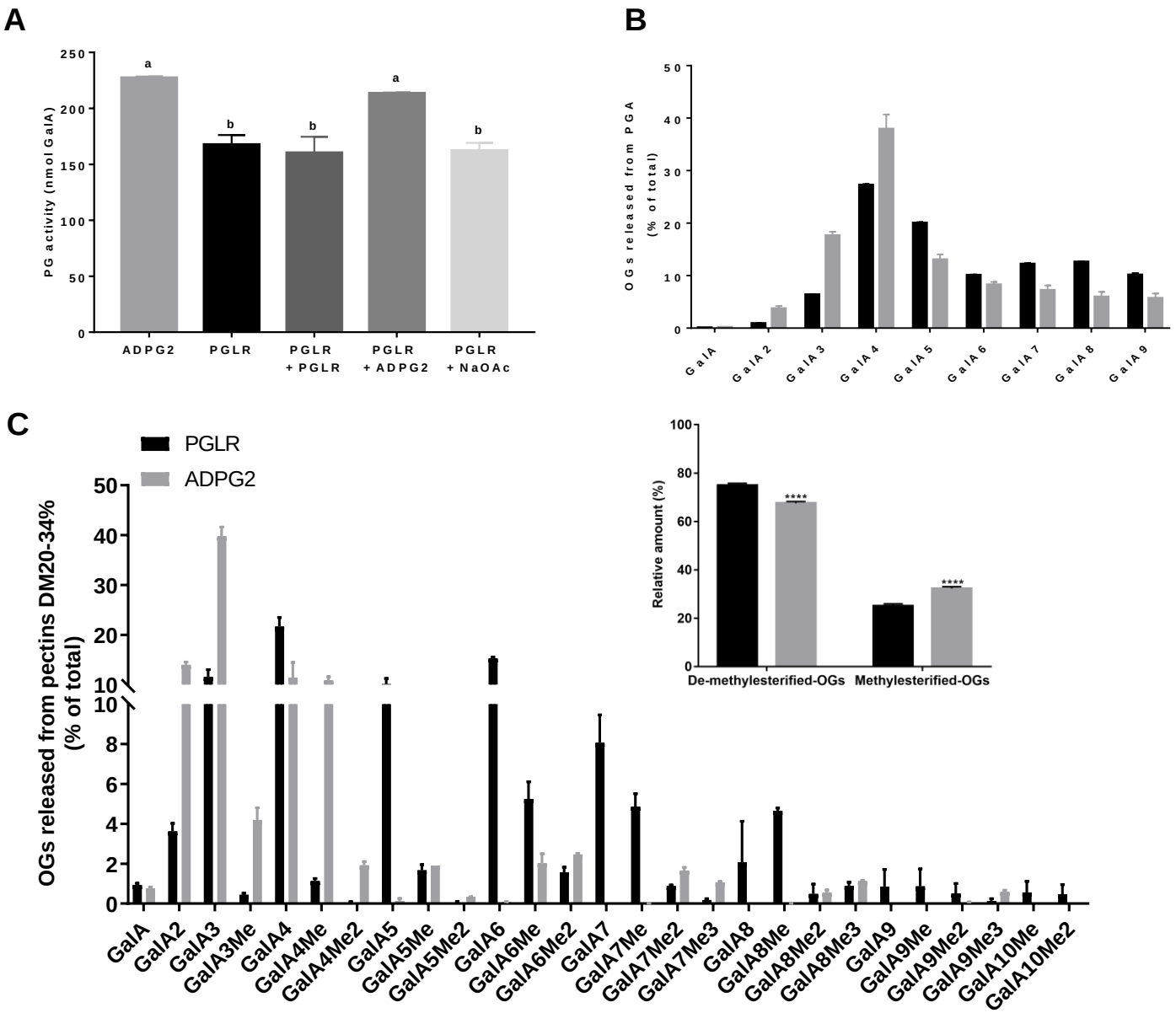

Fig 4. PGLR and ADPG2 release distinct OGs.

A) Activity tests performed on PGA (DM 0) after 1 hour digestion by ADPG2, PGLR and by adding PGLR or ADPG2 for 1 hour after a first digestion by PGLR. NaOAc (sodium acetate): negative control. B) Oligoprofiling of OGs released after 1 hour digestion of PGA by PGLR (black) or ADPG2 (grey) at 40°C, pH 5.2. C) Oligoprofiling of OGs after overnight digestion of pectins DM 20-34% by PGLR (black) or ADPG2 (grey) at 40°C, pH 5.2. Inset: Cumulative OGs released by PGLR and ADPG2 after over-night digestion on pectins DM 20-34% at 40°C, pH 5.2. Two-way ANOVA with Sidask's multiple comparison test, P value ****<0.0001.

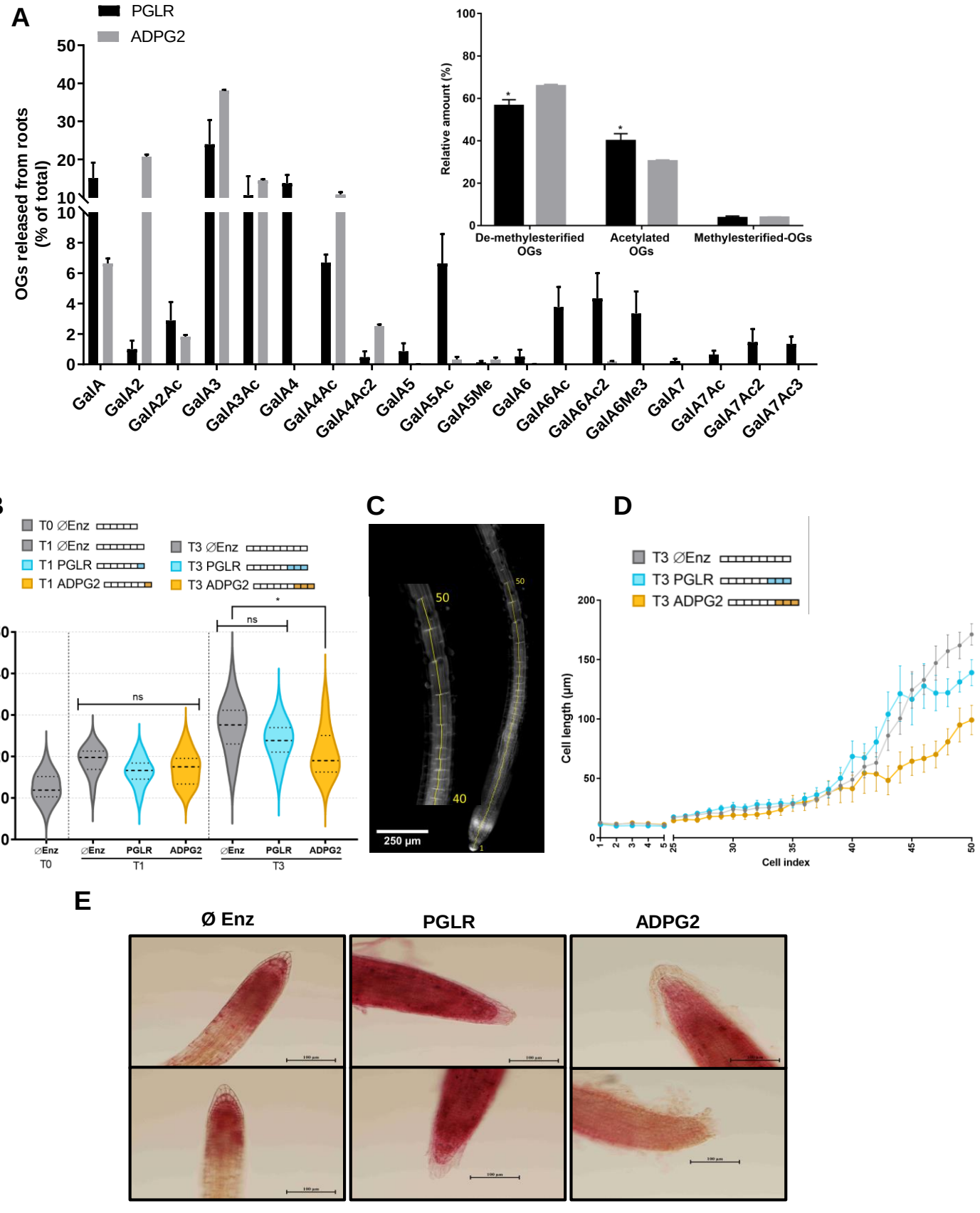

Fig 5. PGLR and ADPG2 are active on roots pectins and have distinct effects of root length

A) Oligoprofiling of OGs after digestion of roots cell wall by PGLR (black) and ADPG2 (grey) at 40°C, pH 5.2 after over-night digestion, (Inset: Cumulative OGs released by PGLR (black) and ADPG2 (grey) after over-night digestion of roots cell walls at 40°C, pH 5.2). Two-way ANOVA with Sidask's multiple comparison test, P value *0.0290. B) Effects of the exogenous application of PGLR and ADPG2 on total root length of Arabidopsis seedlings. PGLR and ADPG2 were applied at iso-activities for one or three days on 6-day-old seedlings grown in liquid media. C) Root cell numbering using EGFP-LTI6b reporter lines. D) Effects of 3-day exogenous application of PGLR and ADPG2 on the cell length of the first 50 roots cells of 7-day-old seedlings. E) Effects of 3-day exogenous application of PGLR and ADPG2 on root cap structure of 7-day-old seedlings (2 representative images per condition). Scale bar represents 100 µm.

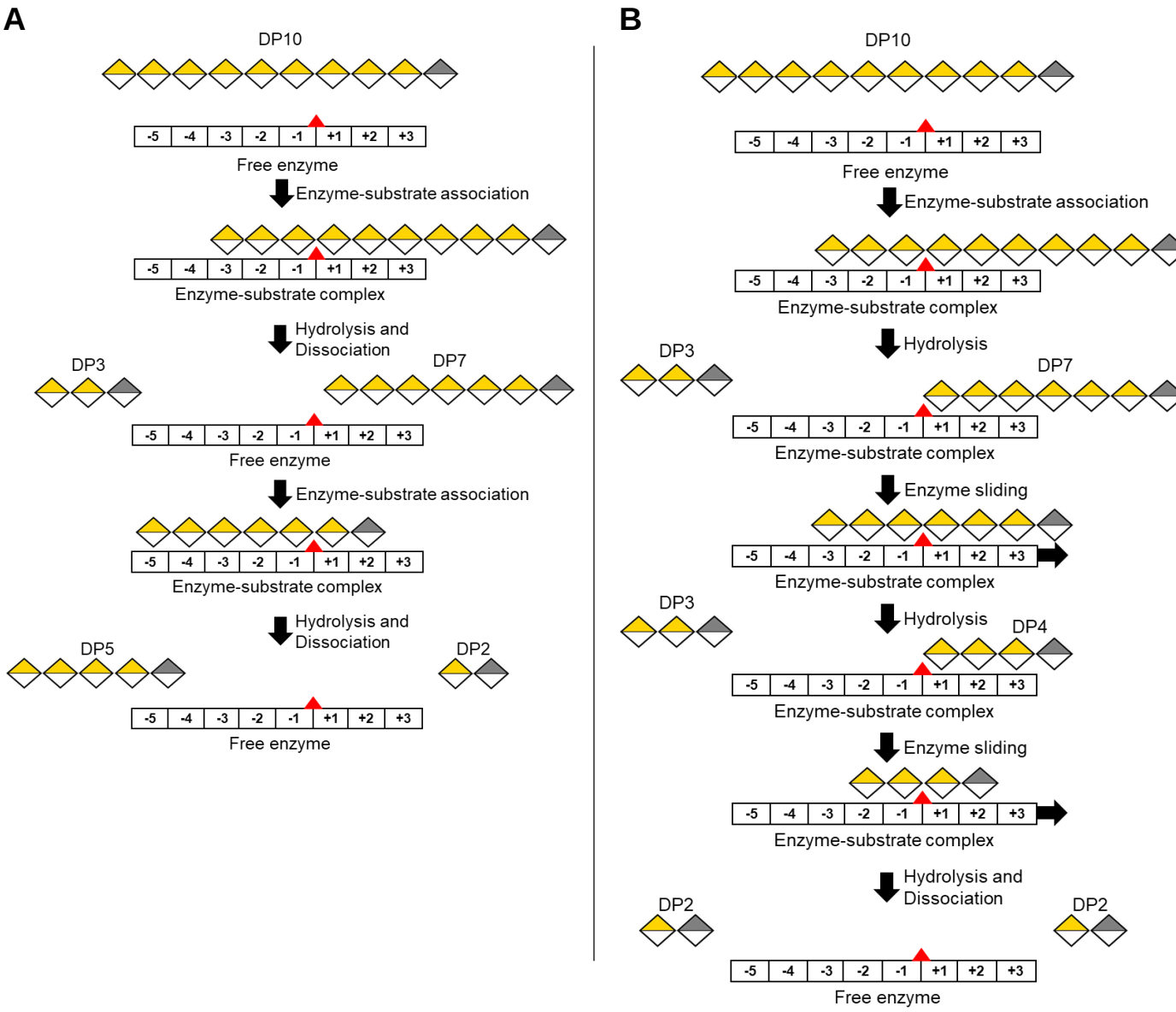

Fig 6. Model of PGLR and ADPG2 processivity

A) PGLR shows low processive dynamics where enzyme-substrate association is followed by hydrolysis and dissociation of the substrate from the enzyme. This low processivity produce OGs of variable DPs. B) ADPG2 sliding motion after forming enzyme-substrate complex allows multiple substrate hydrolysis while staying attached to the substrate showing highly processive dynamics. Processive enzymes can produce small DP OGs. Galacturonic acid are yellow colored. Galacturonic acid reducing end is grey colored. PG subsites are indicated by numbers. Red triangle represents the hydrolysis site.

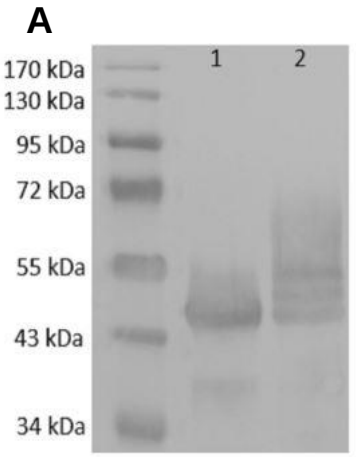

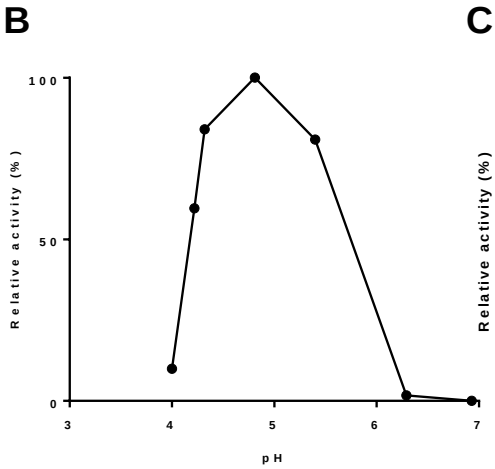

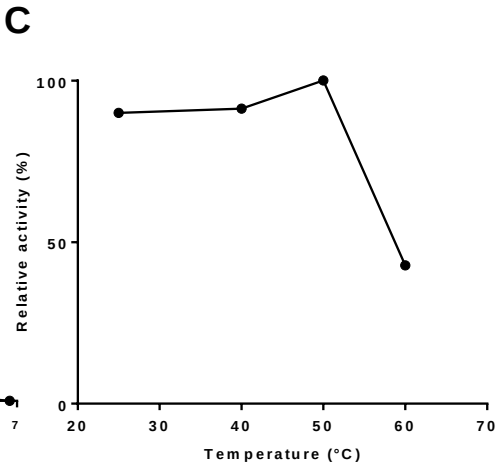

D

Kinetic parameters	PGLR	ADPG2
Km (mg.ml^{-1})	14.6	3.3
Vmax (nmol of GalA.min^{-1}.µg^{-1})	30.8	915.9
Kcat (s^{-1})	22.3	119554

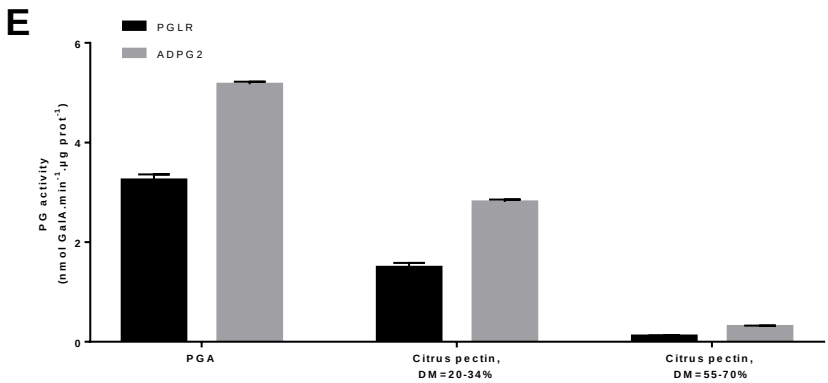

Extended Data Fig 1: Purification and biochemical characterization of ADPG2

A) Western blot analysis of ADPG2 with anti-His antibodies on de-glycosylated form of ADPG2 obtained after digestion by PNGase F (1) and non-digested native sample (2). B) pH-dependence of ADPG2 activity. The activities were measured after 1 hour of incubation with PGA at 25°C at various pHs. C) Temperature-dependence of ADPG2 activity. The activities were measured after 1 hour of incubation with PGA at pH 5.2 at various temperature. D) Determination of Km, Vmax and Kcat for ADPG2 and PGLR. Activity was assessed using various concentrations of polygalacturonic acid (PGA) at 25°C and pH 5.2 using the 3,5-dinitrosalicylic acid method. E) Substrate specificity of PGLR and ADPG2. Activity was measured at 50°C and pH 5.2 during 1 hour using substrates of increasing degrees of methylesterification.

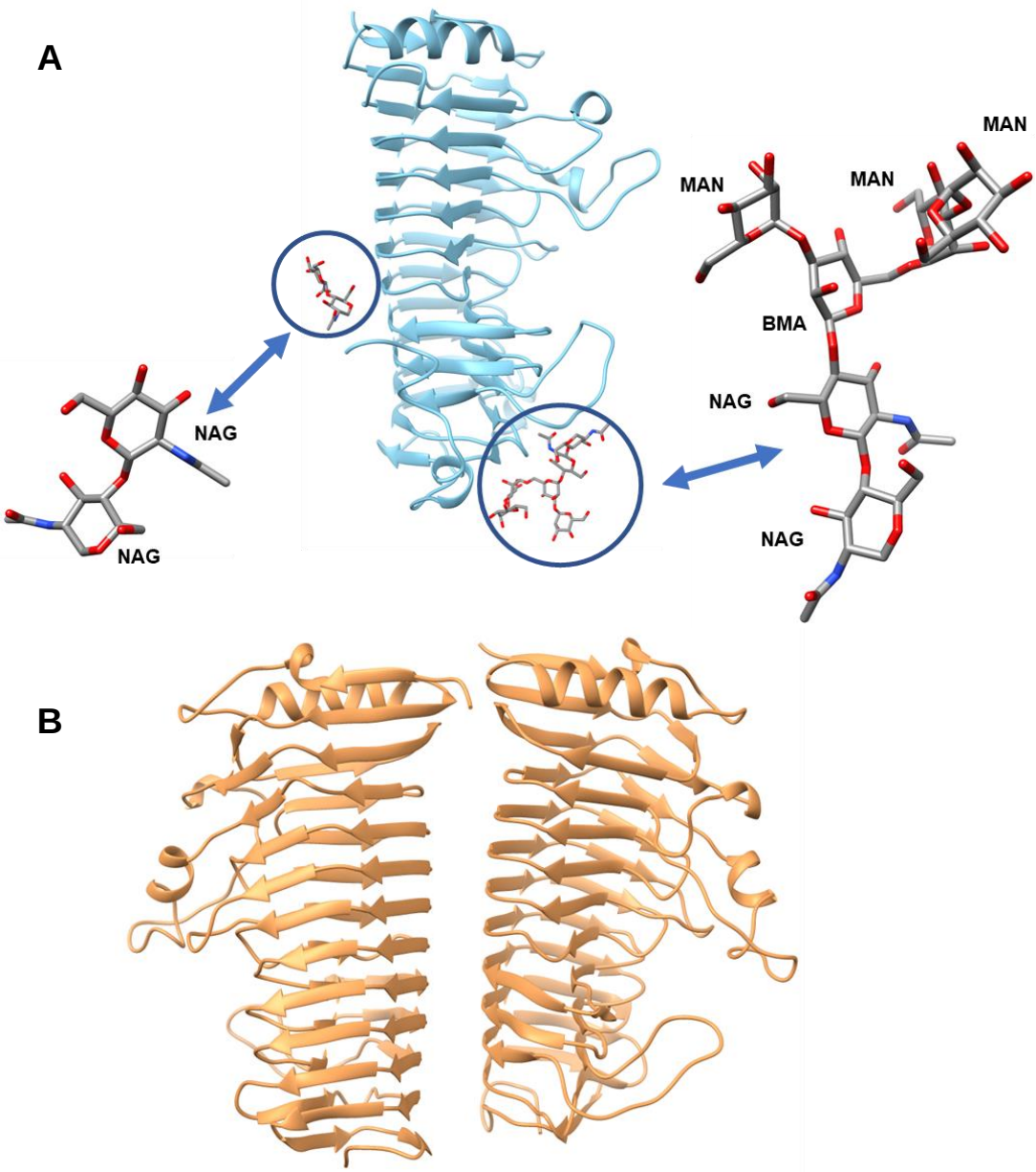

Extended Data Fig 2. Crystallised PGLR and ADPG2 in asymmetric unit and glycosylation sites
A) Ribbon diagram of the PGLR structure containing 1 molecule in the asymmetric unit. PGLR harboured two N-glycosylation sites: Asn255- linked NAG-NAG and Asn313-linked NAG–NAG–BMA–MAN–MAN–MAN. NAG; N-acetylglucosamine, BMA; β-mannose, MAN α-mannose. B) Ribbon diagram of the ADPG2 structure containing 2 molecules in the asymmetric unit.

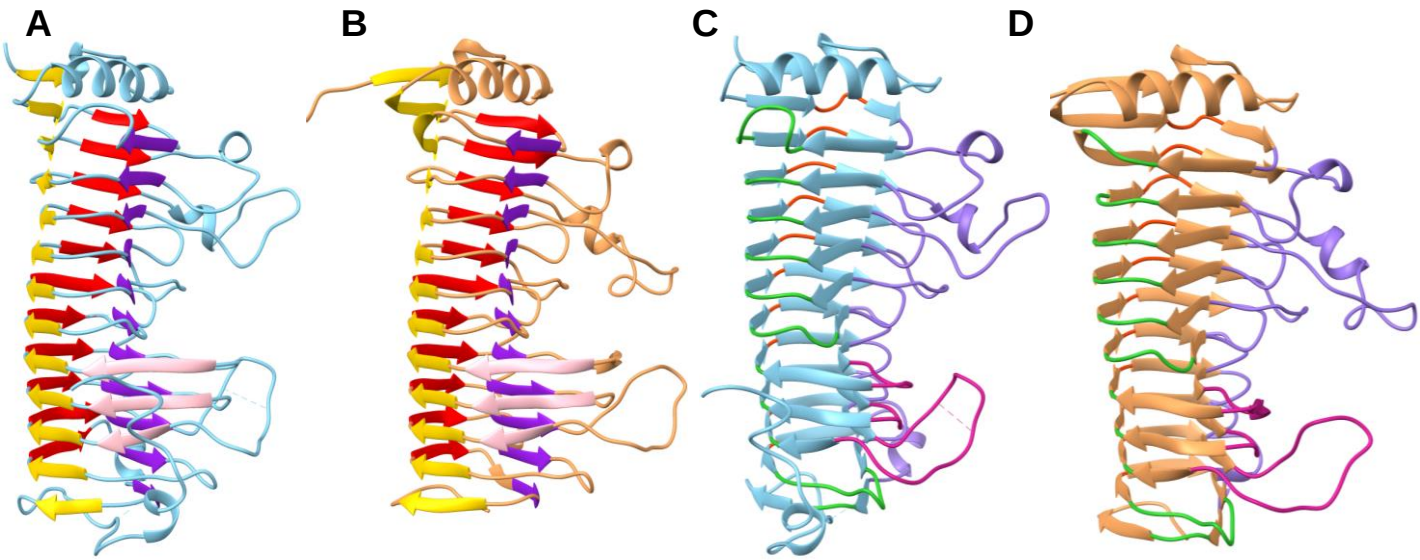

Extended Data Fig 3. PGLR and ADPG2 represent right-handed parallel β-helical structure
Ribbon structure representing β-sheets (PB1-purple, PB1a-pink, PB2-yellow and PB3-red) for PGLR (A) and ADPG2 (B). Ribbon structure representing T-turns (T1-lime green, T1a-violet red, T2- orange red, T3 medium purple) for PGLR (C) and for ADPG2 (D). β-strands and T-turns are named according to Petersen et al. 1997

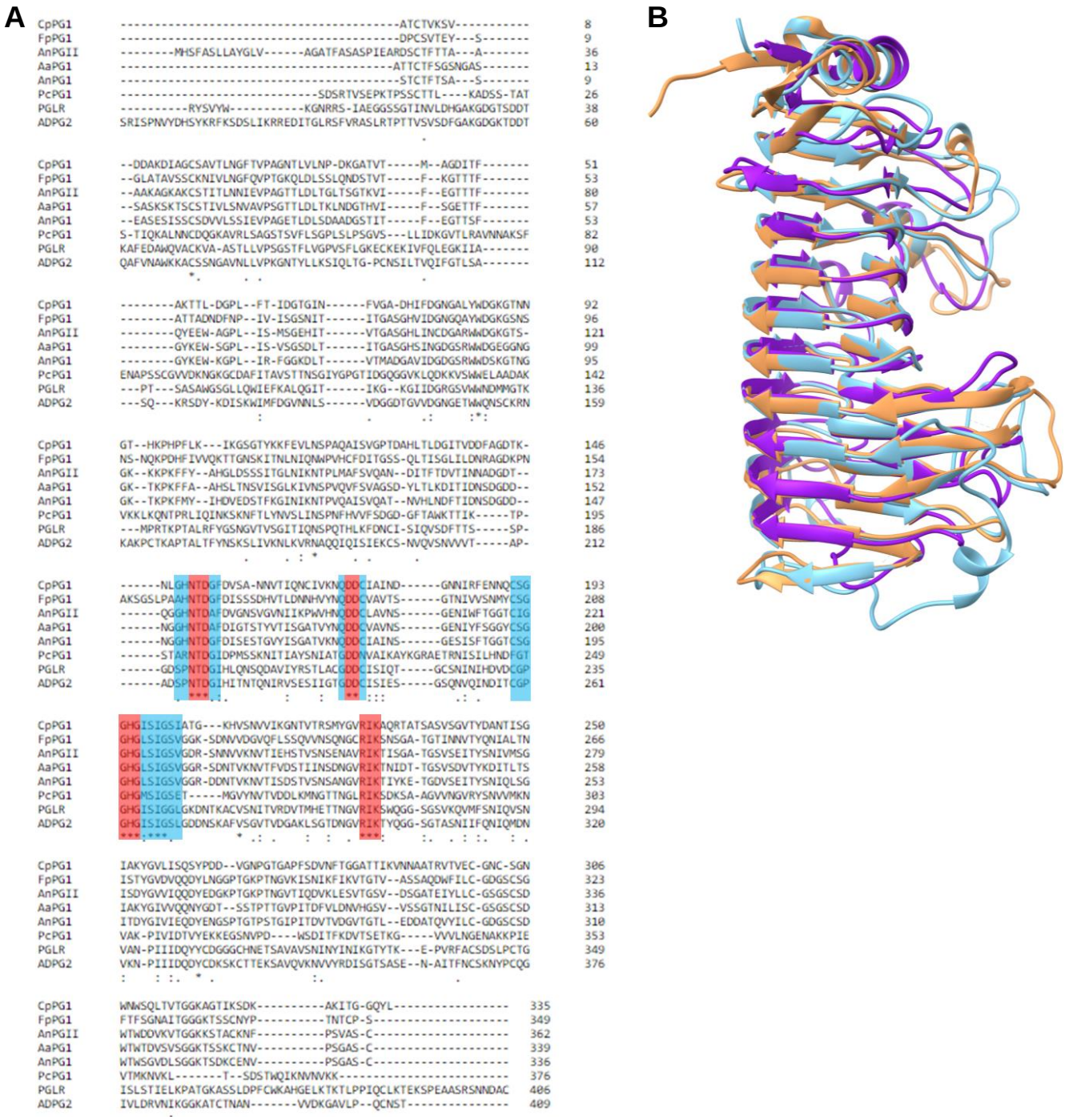

Extended Data Fig 4. PGLR and ADPG2 sequence and structure identity with selected fungal enzymes
A) Sequence alignment of PGLR and ADPG2 with characterized fungal PGs. Selected PGs; *Pectobacterium carotovorum* PG1 (PcPG1, PDB: 1BHE), *Aspergillus niger* PGI (AnPGI, PDB: 1NHC) and PGII (AnPGII PDB: 1CZF), *Fusarium phyllophilum* PG1 (FpPG1, 1HG8), *Aspergillus aculeatus* (AaPG1, PDB: 1IB4) and *Chondrostereum purpureum* (CpPG1, PDB: 1KCD). The aa of the active are red-boxed while and the conserved aa are blue-boxed; The alignment was performed using ClustalO. B) Superimposition of PGLR, ADPG2 and AaPG1 structures[11].

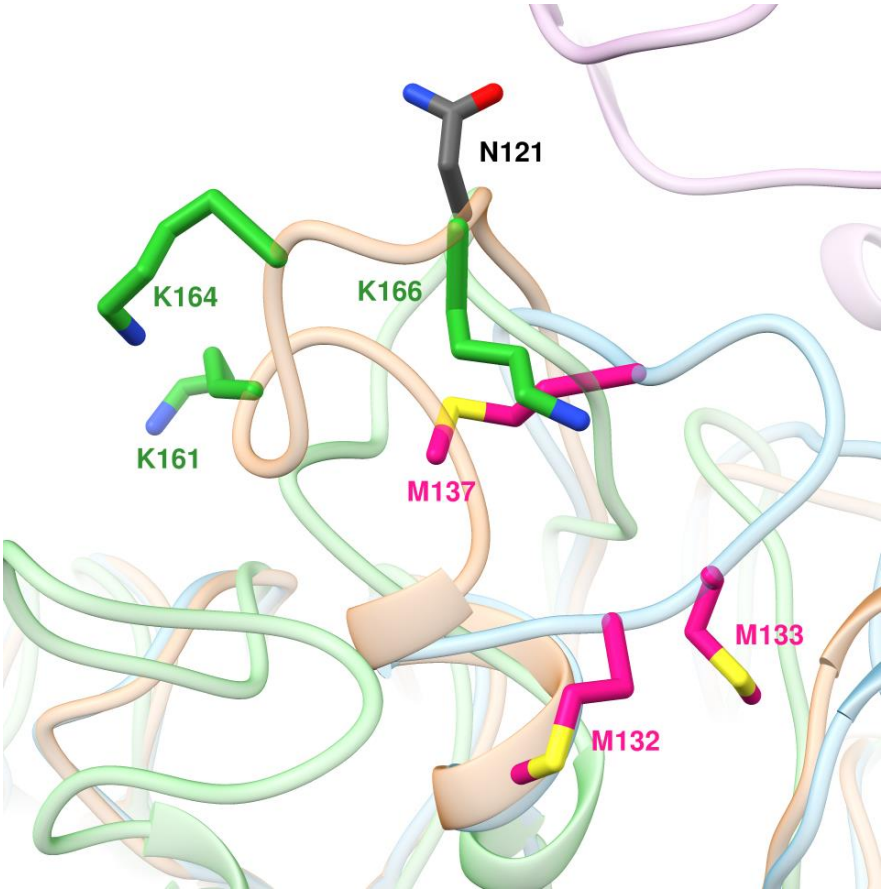

Extended Data Fig 5. PGLR and ADPG2 N-terminal loops
In PvPGIP2-FpPG1 interaction N-terminal loop with N121 play a key role in PG-PGIP interaction (FpPG1 aa in grey). In PGLR (blue) this loop is rich in methionine (pink) while ADPG2 loop (in brown) is rich in lysine (green) residues. PvPGIP2 is plum-colored.

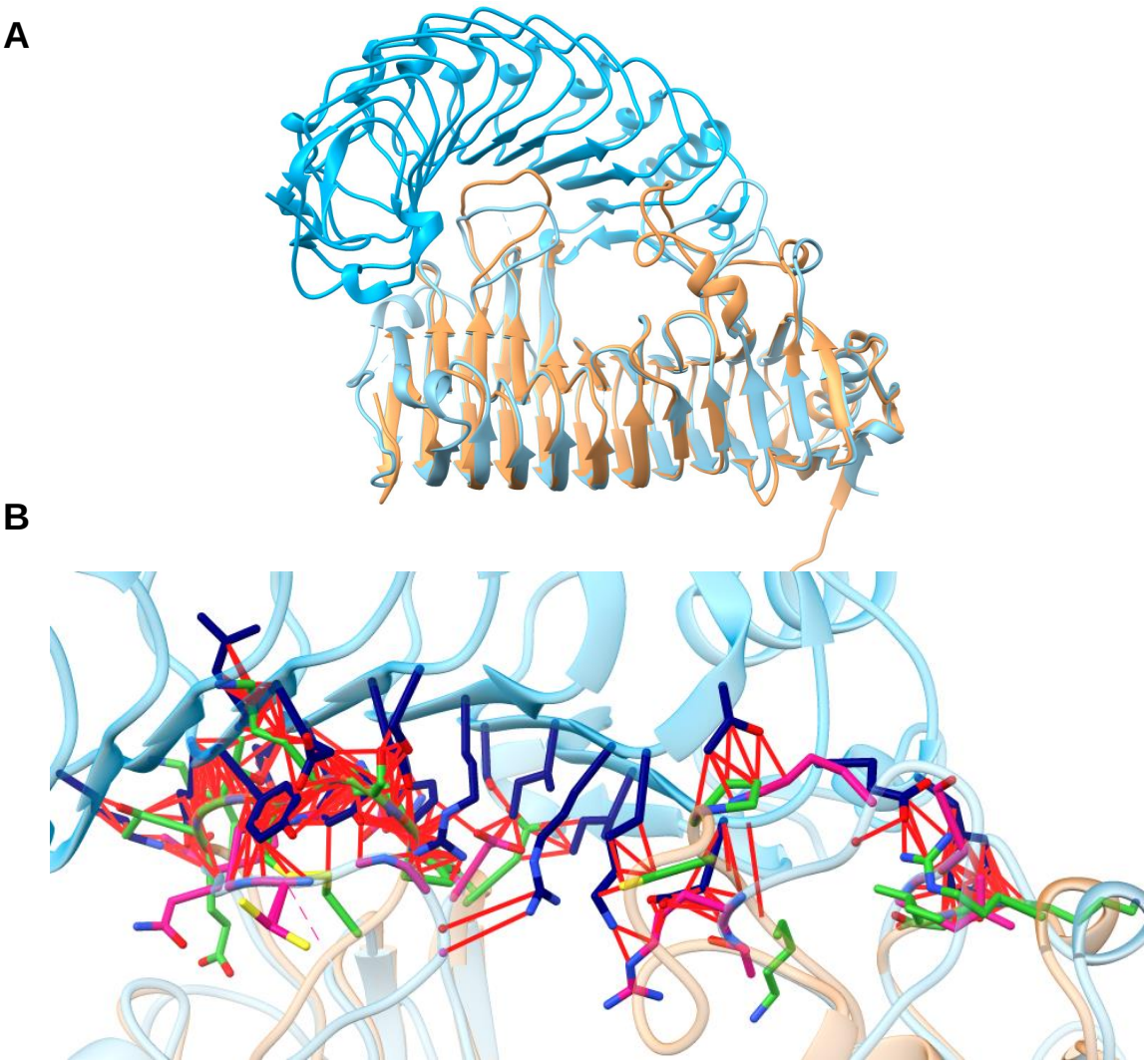

Extended data Fig 6. Structural determinants of the absence of interaction between AtPGIP2 and PGLR-ADPG2 A) Ribbon representation of AtPGIP2 (dark blue) in interaction with PGLR (blue) and ADPG2 (brown). B) Interaction of AtPGIP2 with PGLR and ADPG2. The model of AtPGIP2 was superimposed onto PvPGIP2. Amino acids of AtPGIP2 (dark blue), PGLR (pink) and ADPG2 (green) included in clashes closer than 0.6 Å are shown. The red lines represent atoms overlap of minimum 0.6 Å.

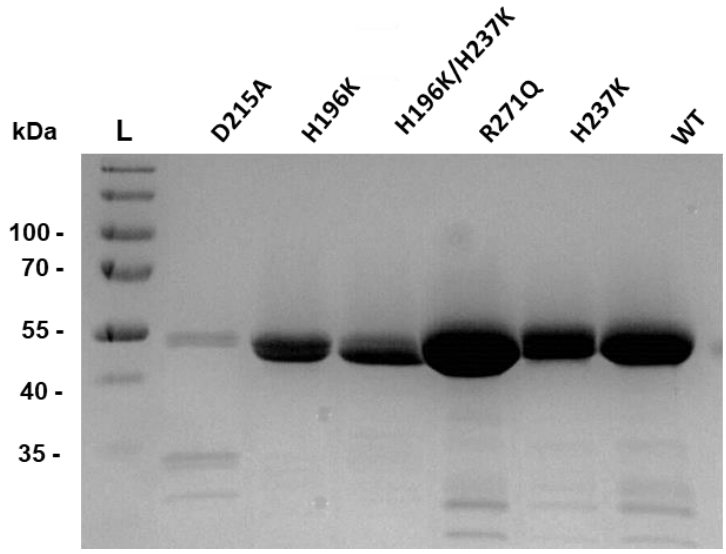

Extended data Fig 7. SDS-PAGE representing the wild type and mutants of PGLR
PGLR and its mutants were purified with His-tag using 1 mL Ni-NTA colon. Proteins were resolved on a 12% polyacrylamide gel and were stained by Coomassie blue. L-ladder.

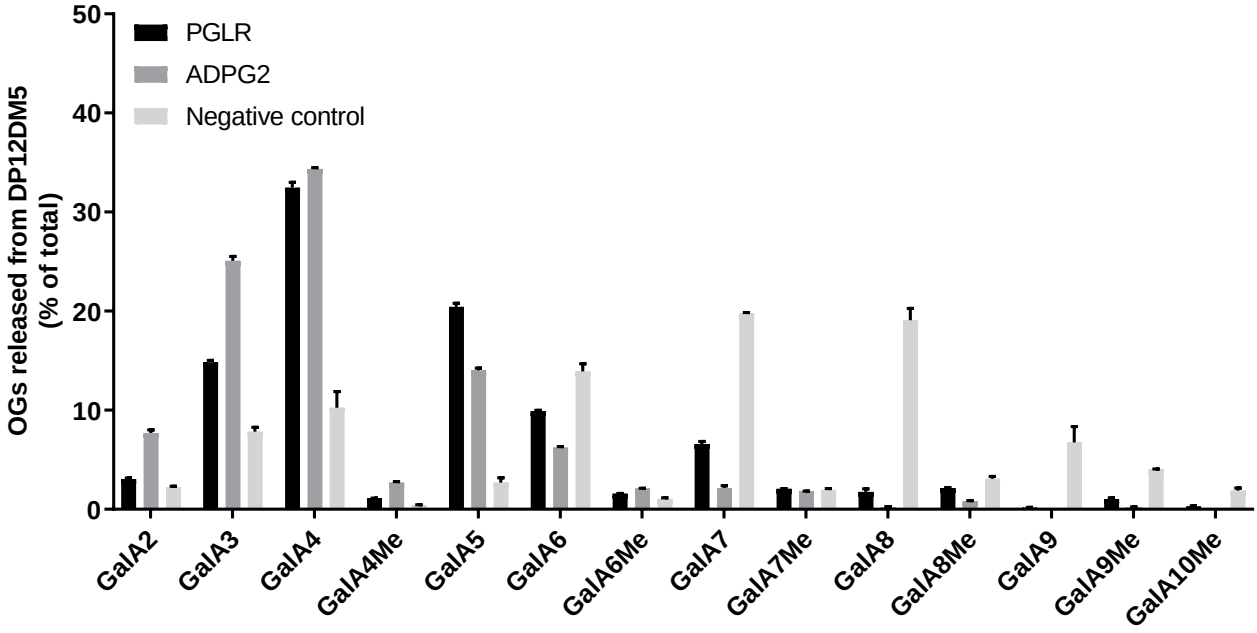

Extended data Fig 8. Oligogalacturonides produced by PGLR and ADPG2 from pectins of DP12DM5
Oligoprofiling of OGs after over-night digestion of DP12DM5 (degree of polymerization centered on 12 and degree of methylesterification centred on 5) pectins by PGLR and ADPG2 at 40°C, pH5.Negative control: undigested DP12DM5 pectins.

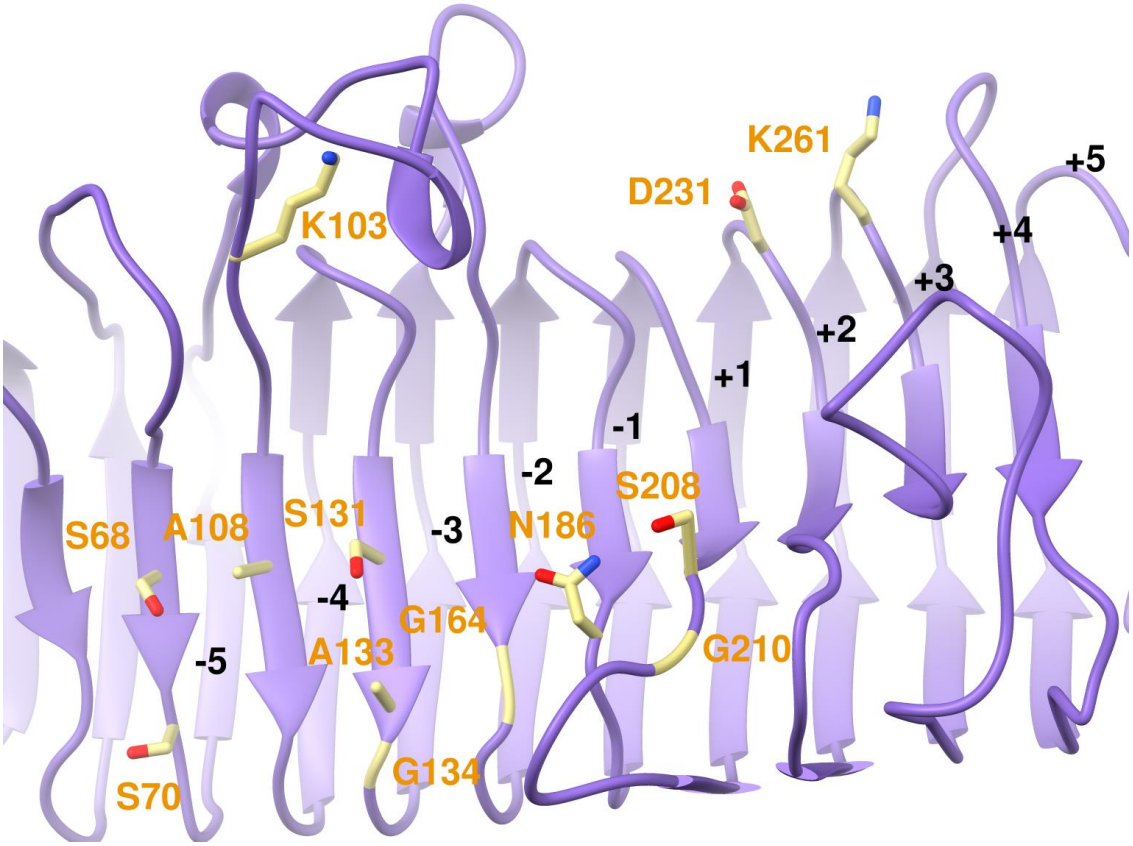

Extended data Fig 9. Structure of subsites of AaPG1
Structure of the -5/+5 subsites of AaPG1 (purple with khaki labelled aa).

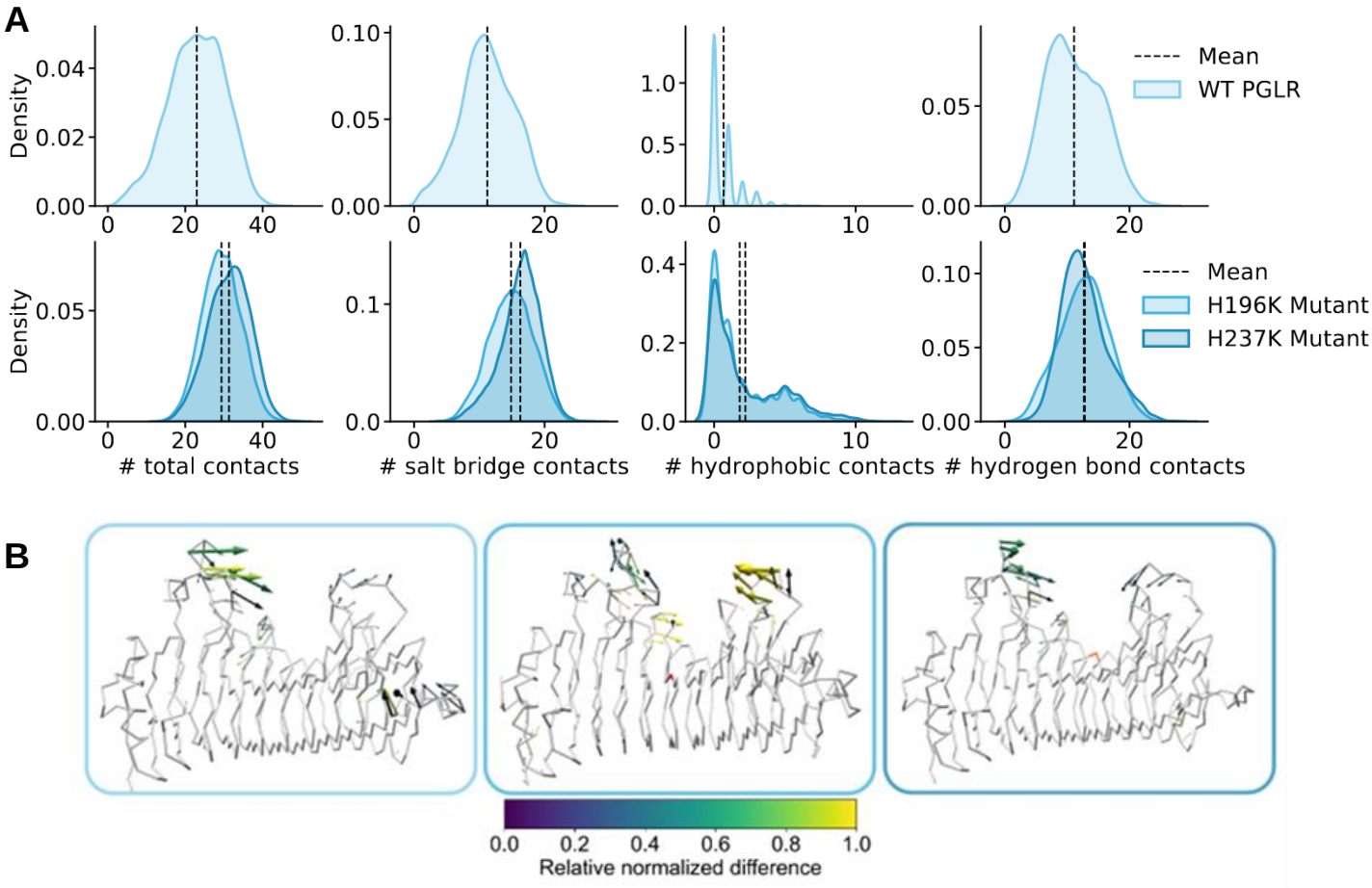

Extended data Fig 10. PGLR H196K and H237K mutants contact calculations

A) Probability density distributions for the number of contacts that occur between WT PGLR (light blue), H196K (medium blue) and H237K mutants (dark blue) and their fully de-methylesterified decasaccharides, within a cutoff of 4.0 Å. Black dashed lines indicate mean values. B) Normalized porcupine plots illustrating the largest motions of protein alpha-carbon atoms represented by the first eigenvector of a principal component analysis, for WT PGLR (light blue; left), H196K (medium blue; middle) and H237K (dark blue; right); complexed to fully de-methylesterified decasaccharides (pattern 1). Arrows indicate direction and relative normalized magnitude of movement, from 0 (dark blue) to 1 (yellow).

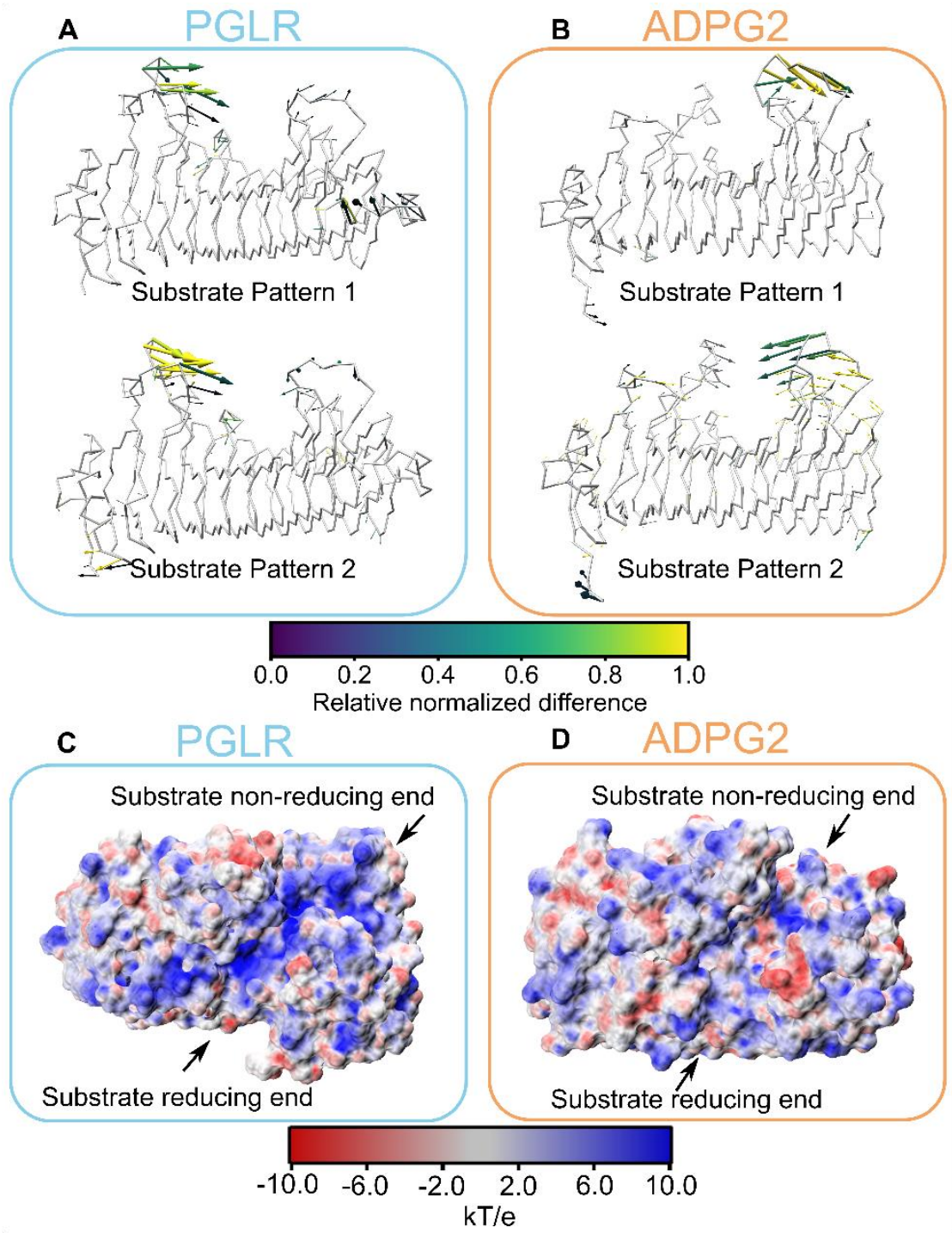

Extended data Fig 11.

A) Normalized porcupine plots illustrating the largest motions of protein alpha-carbon atoms represented by the first eigenvector of a principal component analysis, for WT PGLR with a fully demethylesterified decsaccharide (pattern 1) (top) and a 60% methylesterified decsaccharide (pattern 2, bottom). Arrows indicate direction and relative normalized magnitude of movement, from 0 (dark blue) to 1 (yellow). B) Normalized porcupine plots illustrating the largest motions of protein alpha-carbon atoms represented by the first eigenvector of a principal component analysis, for WT ADPG2 with a fully demethylesterified decsaccharide (pattern 1, top) and a 60% methylesterified decsaccharide (pattern 2, bottom). Arrows indicate direction and relative normalized magnitude of movement, from 0 (dark blue) to 1 (yellow). C) WT PGLR protein surface electrostatic potential projected on the protein's molecular surface, coloured from -10 kT/e (red) to 10 kT/e (blue). The non-reducing (subsite -5) and reducing (subsite +5) ends are labelled as appropriate. D) WT ADPG2 protein surface electrostatic potential projected on the protein's molecular surface, coloured from -10 kT/e (red) to 10 kT/e (blue). The non-reducing (subsite -5) and reducing (subsite +5) ends are labelled as appropriate.

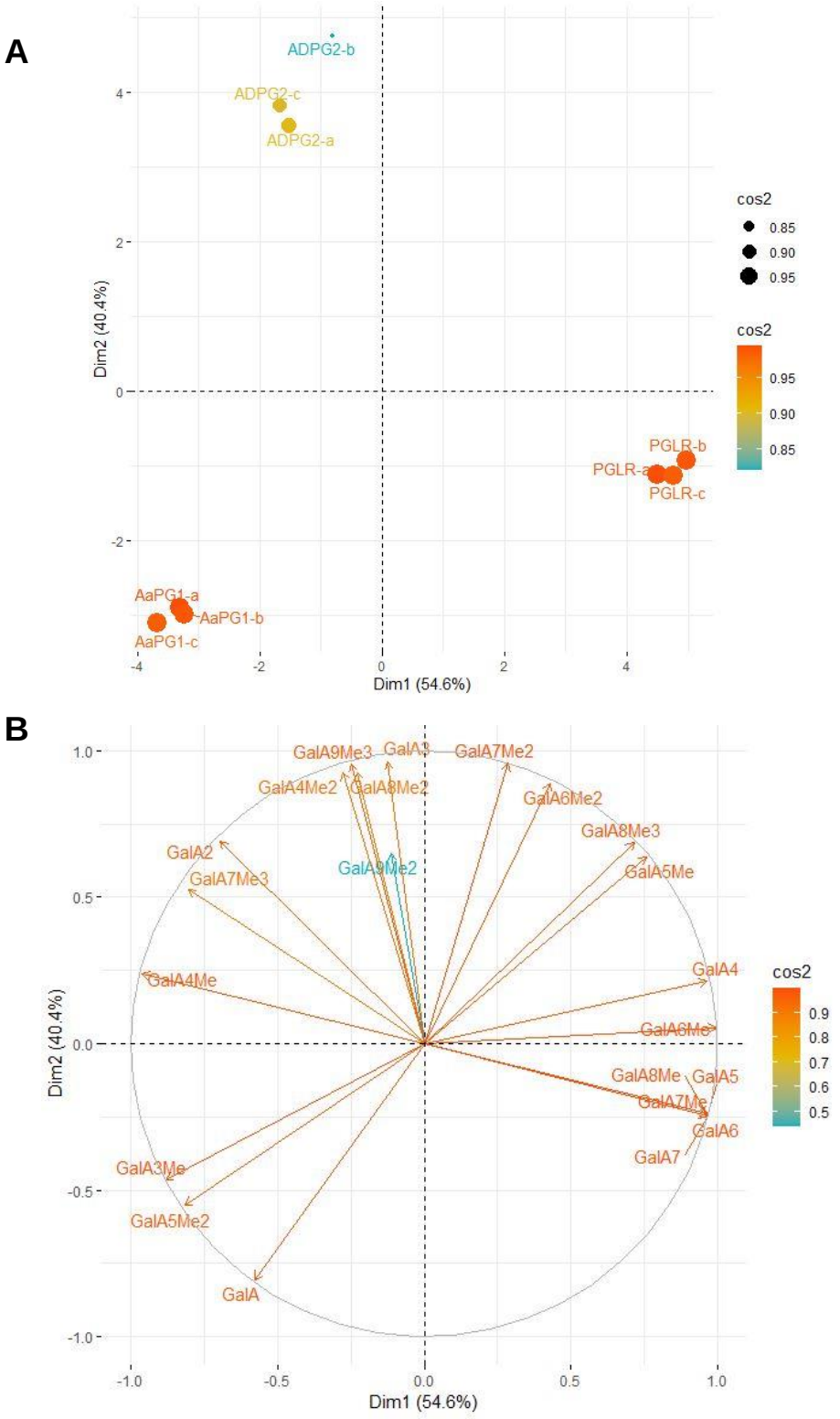

Extended data Fig 12. PCA of OGs produced by PGLR, ADPG2 and AaPG1

A) Score plot of Principal Component Analysis (PCA) of oligogalaturonides released from pectins DM 20-34% by PGLR, ADPG2 and AaPG1. a, b, c represent biological repetitions. B) Loading plot. The oligogalacturonides released after overnight digestions of pectins DM 20-34% by PGLR, ADPG2 and AaPG1 were analysed by PCA using R-package (FactoMineR and Factoextra).

Enzyme	Gene ID	Forward 5'- 3'	Reverse 3'- 5'
ADPG2	At2g41850	*TCTAA*GAATTC*A*CTCAAGAATCAGCCCTAATGTATATGACCA	*TGCAC*GCGGCCGC*A*AGTGGAGTTGCACTGAGGCA
PGLR D215A	At5g14650-D215A	GTTTGGATGGAAATGCA**AGC**GTCACCACAAGCC	GGCTTGTGGTGAC**GCT**TGCATTTCCATCCAAAC
PGLR H196K	At5g14650-H196K*	CCTGGGAGTTTTGCAA**CCT**AATACCGTCAGTG	CACTGACGGTATT**AAG**TTGCAAAACTCCCAGG
PGLR H237K	At5g14650-H237K*	CCAATGGAAATACC**CCT**ACCTGGACCACAATC	GATTGTGGTCCAGGT**AAG**GGTATTTCCATTGG
PGLR R271Q	At5g14650-R271Q	CTTGCCAAGACTTGAT**CTG**GACACCGTTTGTAG	CTACAAACGGTGTC**CAG**ATCAAGTCTTGGCAAG

* At5g14650 H196K-H237K single and double mutants were made using these primers.

Extended data Table 1. Primers for cloning mutated forms of PGLR and ADPG2 into pPICzαB expression vectors.

Table with primers used for the cloning of coding sequences into pPICzαB. Restriction enzymes sites for EcoRI, NotI are underlined, added bases are written in *italics*. Mutation bases are **bolded**.